REP

AD-A226 330

1. AGENCY USE ONLY (Leave blank) | August 1989 | REPORT TYPE AND DATES COVERED: Final Report/15 Dec 85-14 Jan 90

4. TITLE AND SUBTITLE

Formation and Stability of Partially-Neutralized Plasma Clumps

5. FUNDING NUMBERS

61102F/2301/A7

6. AUTHOR(S)

John Guillory, Ren L. Yao, Charles D. Striffler, and Martin Reiser

7. PERFORMING ORGANIZATION NAME(S) AND ADDRESS(ES)

University of Maryland
Laboratory for Plasma Research
College Park, MD 20742

8. PERFORMING ORGANIZATION REPORT NUMBER

AFOSR-TR- 90 0912

9. SPONSORING/MONITORING AGENCY NAME(S) AND ADDRESS(ES)

AFOSR/NP
Bolling AFB DC 20332-6448

10. SPONSORING/MONITORING AGENCY REPORT NUMBER

AFOSR-86-0055

11. SUPPLEMENTARY NOTES

Approved for public release; distribution is unlimited.

12a. DISTRIBUTION/AVAILABILITY STATEMENT

12b. DISTRIBUTION CODE

13. ABSTRACT (Maximum 200 words)

In experiments in which an intense relativistic electron beam is injected into an evacuated drift tube with a localized gas cloud located near the anode, ions with energies several times the electron beam energy have been observed. These experiments have been simulated using a particle-in-cell code which realistically models ionization of the gas. It was found that when the injected electron beam current exceeds the space-charge limiting current, ions are accelerated to energies several times the electron beam energy by coherent motion of the ions and the intense virtual cathode electric fields. The dependence of the peak ion energy on the system parameters as observed in the simulations is also discussed. For the parameter regimes investigated with beam energies up to 3 MV, beam currents up to 35 kA, gas pressures up to 600 mTorr, and gas cloud widths up to 6 cm, peak ion energies of 5-6 times the electron beam energy have been observed. See R. L. Yeo and C. D. Striffler, "Numerical simulation of collective ion acceleration in an intense electron beam-localized gas cloud system," J. Appl. Phys. 67 (4), 15 Feb 90, p. 1650.

14. SUBJECT TERMS

neutralized plasma clumps, ionization, photoionization

15. NUMBER OF PAGES
51

16. PRICE CODE

17. SECURITY CLASSIFICATION OF REPORT	18. SECURITY CLASSIFICATION OF THIS PAGE	19. SECURITY CLASSIFICATION OF ABSTRACT	20. LIMITATION OF ABSTRACT
UNCLASSIFIED	UNCLASSIFIED	UNCLASSIFIED	UL SAR

GENERAL INSTRUCTIONS FOR COMPLETING SF 298

The Report Documentation Page (RDP) is used in announcing and cataloging reports. It is important that this information be consistent with the rest of the report, particularly the cover and title page. Instructions for filling in each block of the form follow. It is important to ***stay within the lines*** to meet ***optical scanning requirements.***

Block 1. Agency Use Only *(Leave blank)*.

Block 2. Report Date. Full publication date including day, month, and year, if available (e.g. 1 Jan 88). Must cite at least the year.

Block 3. Type of Report and Dates Covered. State whether report is interim, final, etc. If applicable, enter inclusive report dates (e.g. 10 Jun 87 - 30 Jun 88).

Block 4. Title and Subtitle. A title is taken from the part of the report that provides the most meaningful and complete information. When a report is prepared in more than one volume, repeat the primary title, add volume number, and include subtitle for the specific volume. On classified documents enter the title classification in parentheses.

Block 5. Funding Numbers. To include contract and grant numbers; may include program element number(s), project number(s), task number(s), and work unit number(s). Use the following labels:

C	- Contract	PR	- Project
G	- Grant	TA	- Task
PE	- Program Element	WU	- Work Unit Accession No.

Block 6. Author(s). Name(s) of person(s) responsible for writing the report, performing the research, or credited with the content of the report. If editor or compiler, this should follow the name(s).

Block 7. Performing Organization Name(s) and Address(es). Self-explanatory.

Block 8. Performing Organization Report Number. Enter the unique alphanumeric report number(s) assigned by the organization performing the report.

Block 9. Sponsoring/Monitoring Agency Name(s) and Address(es). Self-explanatory.

Block 10. Sponsoring/Monitoring Agency Report Number. *(If known)*

Block 11. Supplementary Notes. Enter information not included elsewhere such as: Prepared in cooperation with...; Trans. of...; To be published in.... When a report is revised, include a statement whether the new report supersedes or supplements the older report.

Block 12a. Distribution/Availability Statement. Denotes public availability or limitations. Cite any availability to the public. Enter additional limitations or special markings in all capitals (e.g. NOFORN, REL, ITAR).

DOD	- See DoDD 5230.24, "Distribution Statements on Technical Documents."
DOE	- See authorities.
NASA	- See Handbook NHB 2200.2.
NTIS	- Leave blank.

Block 12b. Distribution Code.

DOD	- Leave blank.
DOE	- Enter DOE distribution categories from the Standard Distribution for Unclassified Scientific and Technical Reports.
NASA	- Leave blank.
NTIS	- Leave blank.

Block 13. Abstract. Include a brief *(Maximum 200 words)* factual summary of the most significant information contained in the report.

Block 14. Subject Terms. Keywords or phrases identifying major subjects in the report.

Block 15. Number of Pages. Enter the total number of pages.

Block 16. Price Code. Enter appropriate price code *(NTIS only)*.

Blocks 17. - 19. Security Classifications. Self-explanatory. Enter U.S. Security Classification in accordance with U.S. Security Regulations (i.e., UNCLASSIFIED). If form contains classified information, stamp classification on the top and bottom of the page.

Block 20. Limitation of Abstract. This block must be completed to assign a limitation to the abstract. Enter either UL (unlimited) or SAR (same as report). An entry in this block is necessary if the abstract is to be limited. If blank, the abstract is assumed to be unlimited.

FINAL REPORT

FORMATION AND STABILITY OF PARTIALLY-NEUTRALIZED PLASMA CLUMPS

Contract AFOSR-86-0055

August 1990

John Guillory

Ren L. Yao

Charles D. Striffler

Martin Reiser

Laboratory for Plasma Research

University of Maryland, College Park, Maryland 20742

SUMMARY

This report covers the research performed under AFOSR contract #86-0055. The work considers the formation and stability of partially neutralized plasma clumps that result when an intense electron beam is passed through a localized plasma source. The main results are:

The injection of an intense electron beam into a localized gas cloud can lead to the acceleration of a 'plasma clump' from the downstream side of the gas into vacuum, with a density comparable to the beam density and at a speed corresponding to beam electron energies and ion mass. This is the expected situation provided the degree of ionization in the gas remains low. Extraction of the ions by the axial electric field as they are produced at a low pressure helps maintain this $n_i < n_b$ situation, and rapid expulsion of newly-created electrons keeps $n_e \ll n_b$ in the gas while $n_i < n_b$ there. If the cathode is hot enough to emit ionizing radiation, the gas should be shielded (or shadowed) from it in order to avoid photoionization.

If, as at higher pressures, n_i builds up to exceed n_b, it is predicted that electron density comparable to n_b or greater can build up in the source gas, leading to rapid electron heating by the two-stream instability, electron-impact avalanche of the remainder of the gas, and a thermal explosion producing a denser jet of plasma with much larger transverse (thermal) energies than in the case of strictly "electrostatic" acceleration. During the course of beam injection at pressures on the order of 1 Torr and above, both the fast tenuous directed jet and, subsequently, the slower, denser jet of the thermal explosion are predicted, and are seen in a 1D simulation. After beam turnoff, at low pressures, a plasmoid with $n_i \sim n_b$ is seen in the simulations to separate from the source gas and propagate downstream. At higher pressures, simulation shows this being followed, even overtaken, by a thermal-explosion jet in which plasma electrons have been very strongly heated.

The interaction of a propagating, expanding plasmoid with a very tenuous ionized background plasma has also been considered. Electrostatic effects are expected to dominate over collisional or magnetic effects. Enhanced electric field fluctuations in the propagating plasmoid are predicted to raise its transverse electron temperature and thus contribute to its reduction in axially-directed energy flux density due to enhanced radial expansion.

Contents

1 Introduction

This report considers a specific system in which the formation and stability of partially neutralized plasma clumps are studied. An electron beam with peak current of order 20 kA, with a time history corresponding approximately to a 25-ns half-cycle of a sinusoid, with a typical electron energy of 0.5 MeV, and with an expected final radial extent of order 1 cm, is assumed to propagate through a $\sim$1 cm hydrogen gas puff and create a virtual cathode on the vacuum downstream side of the gas puff. The gross beam current greatly exceeds the propagation limit for vacuum in the pipe, so the beam cannot propagate macroscopic distances in the vacuum until it is largely neutralized there by ions accelerated forward from the ionizing gas.

In what follows, we describe both analytic and numerical studies of the initial phase of the process: the ionization dynamics in the gas, the heating of the resulting plasma, the formation of both electrostatically accelerated jets of ions and thermally-produced jets of heated plasma, and a 1-D electrostatic simulation of these processes. Then we describe in a preliminary way the exchange of momentum and energy between a propagating partially-neutralized "plasmoid" of finite extent and low-density background plasma. Some dynamic simulations of the "plasmoid" formation and detachment on beam turnoff have also been completed, and we have made some analytic conclusions regarding the disturbance of low-density background plasma by the dense plasmoid. Many details of two-stream interaction and experimental consequences, and of electrostatic acceleration of an ion front from the source plasma have been reported previously (Ref. 1 and references cited therein).

2 Source Plasma Ionization – Analytic Theory

In order to coordinate closely with our computer simulation and concurrent experimental efforts, we have analyzed the ionization processes in a $\sim$1 cm gas puff ($P \leq 5$ torr) through which an electron beam propagates and from which it extracts ions to form a partially neutralized propagating plasmoid downstream. In describing the electron and ion density buildup by ionization, we have included the effects of electric fields inside the ionizing gas puff, and include ionization by ion-neutral collisions. The gas, puffed transversely across

the electron beam path adjacent to the diode, is exposed to beam electrons and cathode radiation through the anode aperture, approximately 1 cm in diameter.

The simulations realistically model impact ionization of the gas by electrons and ions but neglect photoionization of the gas by cathode radiation. If the injected beam current is much greater than the space-charge limiting current for the system, a virtual cathode forms near the anode plane soon after the beam is injected. If the gas pressure is high enough, the VC moves downstream to the end of the gas region. As it moves downstream we find that ions are accelerated to energies several times the el beam energy by coherent motion of the ions and the intense VC electric fields which follow the VC. We also find that the potential in the gas region becomes positive. Once the VC has reached the end of the gas region (if the pressure is neither too high nor too low) the system reaches a quasi-steady state in which ions are extracted from the gas by the VC electric fields at a constant rate; els are also lost from and propagate downstream at a constant velocity on the order of $(eV_0/m_p)^{1/2}$, where V_0 is the el beam energy and m_p is the ion mass. We also find that the secondary els are also able to escape from the gas region, even though the potential is positive in that region.

In the following sections, we compare the ionization rates for el and ion impact ionization and photoionization during the initial stages of the beam pulse when little or no ionization is present, and during the latter stages when a quasi-steady state has been reached.

We have calculated and compared (a) impact ionization by the 0.5 MeV reflexing electron beam, (b) photoionization by assumed cathode UV radiation, and (c) ionization resulting from collisions of accelerating ions with neutrals. The beam is modeled as a density $n_b(t)$ given by the first half-cycle of a sine wave:

$$n_b(t) = 0.5 \times 10^{13}\mathrm{cm}^{-3}\ \sin(\pi t/50\mathrm{ns}), t < 50\mathrm{ns} \tag{1}$$

2.1 Electron impact ionization

Assuming the beam has spread radially to 1 cm diameter, this corresponds to a peak one-way current of approximately 20 kA for a radially flat beam profile. For H_2, we expect this primary ionization to build plasma density according to

$$\dot{n}_i(\mathrm{cm}^{-3}/\mathrm{ns}) = .34\ P_{torr}\ n_{bmax}(\mathrm{cm}^{-3})\sin(\pi t/50\mathrm{ns}), \tag{2}$$

i.e.,

$$n_i(\mathrm{cm}^{-3}) \sim 5.4 P_{torr} n_{bmax}[1 - \cos(\pi t/50\mathrm{ns})] \tag{3}$$

from primary electron impact ionization, if ion motion is neglected.

2.2 Photoionization

The photoionization rate is essentially independent of the plasma density and hence will be independent of gas density and beam density during all stages of the beam pulse, assuming that the cathode radiation is the same throughout the beam pulse. We see that the photoionization rate is strongly dependent on cathode plasma temperature. If the temperature is sufficiently high, photoionization could produce enough ionization early in the beam pulse to prevent formation of a VC in the gas region. If the VC does form in the gas region, photoionization will contribute to ionization of the gas and the VC will simply move down to the end of the gas region sooner and more quickly than otherwise.

To estimate the photoionization rate, we first suppose the cathode plasma to be a perfect blackbody radiating as a several-eV plasma. The radiation flux over a 2π hemisphere solid angle, from the 15 mm radius cathode (.0707 cm^2), with unit emissivity, would be

$$P(W) = 1.7 \times 10^7 \left(\frac{T_c}{7\mathrm{eV}}\right)^4, \tag{4}$$

with a more or less uniform radiation intensity a distance r (cm) from the cathode center,

$$I_\phi(W/\mathrm{cm}^2) \approx 2.7 \times 10^6 \left(\frac{T_c}{7\mathrm{eV}}\right)^4 \frac{1}{r_{\mathrm{cm}}^2}. \tag{5}$$

The H_2 photoionization cross-section rises quickly from the 13.6 eV photon-energy threshold to peak at $\sigma_{\phi 1} \approx 8$ Mbarns $= 10^{-17}$ cm^2 (Ref. 2). The integrated radiation intensity above 14 eV from a 7 eV blackbody is about 80% of the total flux, so we could multiply I_ϕ by 0.8 and use the peak cross-section. This gives

$$n_e(\mathrm{cm}^{-3}) \sim \frac{2.3 \times 10^{15}}{r^2(\mathrm{cm}^2)} \left(\frac{t}{10\mathrm{ns}}\right) \left(\frac{T_c}{7\mathrm{eV}}\right)^4 P(torr) \tag{6}$$

for constant cathode conditions during the first 10 ns. (For $T_c \approx 7$ eV, this corresponds to several percent ionization of the gas, increasing to ~20% by 50 ns when the beam stops.)

We refine this calculation next by using the model photoionization cross-section for hydrogen

$$\sigma_{\phi i}(\epsilon_\phi) \approx \begin{cases} 0 & \text{for } \epsilon_\phi < \epsilon_i \\ \sigma_0(\epsilon_i/\epsilon_\phi)^3 & \text{for } \epsilon_\phi > \epsilon_i \end{cases} \tag{7}$$

$$\sigma_0 = 0.79 \times 10^{-17}\text{cm}^2, \epsilon_i = 13.6\text{eV} \tag{8}$$

and the blackbody spectrum from a cathode at temperature T_c. From this we calculate the photoionization rate coefficient:

$$\dot{n}_e(\phi i)/n_a = \frac{2\pi\epsilon_i^3}{h^3c^2}\left(\frac{T_c}{r}\right)^2 \sigma_0 \Sigma_{n=1}^{\infty} E_1(n\epsilon_i/T_c) \tag{9}$$

with n integer and $E_1(y)$ the exponential function,

$$E_1(y) \equiv \int_y^\infty \frac{e^{-t}dt}{t}. \tag{10}$$

The sum converges rapidly when T_c is not larger than ϵ_i, and is shown in Fig. 1. Between 3 and 12 eV, an approximate scaling as T^4 is evident. The coefficient multiplying the sum in Eq. (9) is approximately $2 \times 10^9 s^{-1}$. At cathode temperatures below 2 eV, the sum is approximately $(T_c/\epsilon_i)\exp -(\epsilon_i/T_e)$, but the ionization rate then depends sensitively on having the full blackbody tail of the cathode photoemission spectrum. Given such a spectrum, the time to increase the ionization fraction $f_i = n_e/n_a$ to 1% by photoionization alone would be 5 ns at $T_c = 2.7$ eV.

Thus we conclude that, even if the emissivity of the cathode is as low as 0.1 and its temperature as low as 3.5 eV instead of 7 eV, photoionization probably dominates over impact ionization by the 1 MeV beam electrons, when the gas is exposed to hot-cathode UV radiation.

2.3 Ion-neutral collisions

The modeling of avalanche ionization in the quasi-static electric fields of the rising beam has been included in the analytic theory and in the simulation. First, the radial space-charge electric field, E_r, of a 0.5 cm-radius beam with $n_b = 0.5 \times 10^{13}$ cm^{-3} $\cdot$ $\sin(\pi t/50$ ns) would be of order 2 MV/cm $\cdot$ $\sin(t/16$ ns) at the beam edge, if there were no space-charge

neutralization. But in about 10-100 ps, photoionization from an unshielded hot cathode could produce $n_p \sim n_B$ at the entrance side of the gas, so that if the initial plasma electrons are expelled by the fields, charge neutralization is established very early and no such radial field magnitudes would build up. Likewise, inductive fields due to the rise of net current are much reduced by the return current carried by photoionized electrons. But the residual electric field in the gas/plasma may still be great enough to accelerate ions to energies at which their cross-section for ionization of neutrals is quite large.

To estimate the ionization due to accelerating ions of energy ϵ in the source plasma, we use the model cross-section

$$\sigma_i(\mathrm{cm}^2) = \begin{cases} 0.73 \times 10^{-17}[\epsilon(\mathrm{keV})]^{1.03}, & 10\mathrm{eV} < \epsilon < 43\mathrm{keV} \\ 0.73 \times 10^{-14}[\epsilon(\mathrm{keV})]^{-.7985}, & \epsilon > 43\mathrm{keV} \end{cases} \tag{11}$$

for hydrogen. First, we use the preliminary estimate, V_0/ℓ_p (diode voltage over source-plasma length), for the average accelerating electric field, giving $\epsilon \sim eV_0 z/\ell_p$ and, to order of magnitude

$$\dot{n}_i(\mathrm{cm}^{-3}/\mathrm{ns}) \sim 1.63 n_i \left[\frac{V_0}{511\mathrm{kV}}\frac{z}{\ell_p}\right]^{-0.3} P_{\mathrm{torr}} \quad \text{for } z/\ell_p > 0.1. \tag{12}$$

This preliminary estimate corresponds to n_i exponentiating in a time

$$\tau_{av}(\mathrm{ns}) \approx 0.6 \left[\frac{V_0}{511\mathrm{kV}}\frac{z}{\ell_p}\right]^{0.3} P_{\mathrm{torr}}^{-1} \tag{13}$$

in the absence of ion convection and other ionization mechanisms.

As ions are accelerated in the virtual cathode electric field they move into and out of the regions where their impact ionization cross-section is greatest. To improve on the preliminary estimate of the location and extent of hydrogen ionization, and to check the approximate validity of code calculations of ionization, we made a simple model of ion-impact ionization by ions accelerated from rest in a given electric field distribution that was chosen to model the computed field distribution in the gas cloud. A 'weak' E_z field was assumed over a fraction ℓ_1/ℓ_s of the gas, and a stronger E_z field was assumed over the virtual cathode layer of width $\ell_2 \ll \ell_1$ downstream of the ℓ_1 region. This was not a truly self-consistent calculation in that (a) the field was taken as given, and (b) all ion transit-time effects were ignored. In

a constant electric field E_z a proton would leave the gas rather quickly:

$$t_{\ell v}(\mathrm{ns}) \sim 1.3[\ell_p(\mathrm{cm})/E_z(\mathrm{MV/cm})]^{1/2} \tag{14}$$

and on this timescale we ignore changes in the electron beam and the ionization profile. We thus treat the quasi-static problem of determining the z-dependence of ion density for given electron beam density.

In this model, ionization is produced only by beam electrons and by accelerated ions. The ionization rate at position z in the gas is

$$\dot{n}_i(z) = n_0 n_b < \sigma_e v_b > + n_0 n_i(z) < \sigma_i v_i >_z \tag{15}$$

with the cross-section σ_i given as a function of energy (or ion velocity) by Eq. (11).

When the electric field for $0 < z' < z$ has the constant value E_1, ion energy at z is just $e\phi(z) - e\phi(z')$ for ions born at $z' < z$, and $\phi(z) - \phi(z') = -(z - z')E_1$. Since the value of $\dot{n}_i(z = 0)$ is just $n_0 n_b < \sigma_e v_b > \equiv S_0$, we can show that in the interval $z < \ell_1$ the low-pressure equation for $\dot{n}_i(z)/S_0 \equiv R(z)$ is a Volterra integral equation of the second kind,

$$R(z) = 1 + n_0 \int_0^z \sigma_i(\epsilon) R\left(z - \frac{\epsilon}{eE_1}\right) d\left(\frac{e}{eE_1}\right), \tag{16}$$

where ϵ is an energy variable. Letting $u \equiv \epsilon/eE_1$ and $w = z - u$, this can be put in the standard form

$$R(z) = 1 + n_0 \int_0^z S(z - w) R(w) dw \tag{17}$$

with $S(x) \equiv \sigma_i(\epsilon = xeE_1)$.

To first order in $n_0 \sigma_{i,max} \ell_s \lesssim 1$, i.e. for low pressures, the solution of the integral equation can be approximated, using Eq. (11), as

$$R(z) = 1 + \frac{1}{2}(n_0 c_1) x_p^2 + 5(n_0 c_2)(z^{0.2} - x_p^{0.2}) \tag{18}$$

for $z > x_p$, where for H_2,

$$n_0 c_1 \approx 516\ E_1(\mathrm{MV/cm}) P(torr) \tag{19}$$

$$n_0 c_2 \approx 2.0\ P(Torr)\,[E_1(\mathrm{MV/cm})]^{-0.8}, \tag{20}$$

and x_p is the distance required to accelerate an ion to the peak energy of the ionization cross-section, i.e. 43 keV ($x_p = .215$ cm at 0.2 MV/cm). Validity of the expansion requires

the right hand side of Eq. (18) to be of order unity. For expected E_1 fields of order 0.2 MV/cm in the body of the gas cloud, the ionization rate at position z inboard of the 'virtual cathode' at $z = \ell_1 \approx \ell_s$ is given approximately by

$$R(z) = 1 + 2.4(P/e_1) + 36(P/e_1)\left[(e_1 z)^{0.2} - 0.735\right] + O(P^2) \tag{21}$$

times the electron beam ionization rate, with

$$e_1 \equiv E_1/(0.2 \text{ MV/cm}),$$

$0.4 \leq e_1 z \leq e_1 \ell_1$, z in cm and P in Torr.

This result decreases as the accelerating field E_1 is increased, because the peak of the ion-neutral ionization cross-section occurs at rather low energy, 43 keV, compared with the energies achieved by ions accelerated across the gas by the E_1 field strengths anticipated.

One can add uniform photoionization to that by the primary beam electrons without difficulty, just by redefining S_0 to include both sources. The quantity $R(z)$ is then the ratio of total ionization to that by photons plus beam electrons; i.e., $R(z)$ is the ionization enhancement ratio due to accelerated ions.

For higher pressures (above the validity of the first-iterated-kernel expansion), the gas can avalanche due to ionization by accelerated ions. The foregoing treatment is limited to low pressures, at which ions leave as rapidly as they ionize, i.e., the length of gas is less than a typical ionization length. One can show that in this case n_i remains less than n_b if photoionization is ignored, so that the beam is not charge-neutralized, at the low pressures for which Eq. (21) is derived, unless photoionization is significant. The analysis above is also strictly one-dimensional and makes no provision for radial loss of ions.

The mathematical formalism of the foregoing low-pressure model calculation is insensitive to the location or existence of any virtual cathode strong-field region. If the strong-field region is located on the upstream side of the gas (as observed in the computer simulations at early times and low ionization), then the magnitude of the term, S_o, representing direct ionization by the electron beam, is altered, because beam electrons that do escape over the potential barrier and stream through the gas have lower velocity and larger ionization cross-section than would be the case with a virtual cathode at the downstream end.

For 500 keV - 1 MeV electron beams, the ionization due to accelerating ions is about one order of magnitude larger than that by secondary electrons (Ref. 3), and it is the dominant process governing the ionization once photoionization (or any other process) raises n_i to around 10^{13} cm^{-3}. However, the voltage drop across the source plasma may collapse when the avalanche occurs, at first increasing and finally reducing the ion acceleration.

As ionization occurs in the gas, newborn electrons are at first rapidly expelled by the beam space charge, which is not yet fully compensated by the ions being formed. This is the ion-focusing regime (IFR) of beam propagation through the gas puff. If newborn ions are too slow to leave on the timescale of their formation, they would simply accumulate until $n_i = n_b$, at which time the expulsion of newborn electrons would cease. Further accumulation of ions by ionization would then be accompanied by the buildup of retained newborn electrons. This is important because it provides a highly unstable distribution of electron momenta, with a quasi-stationary "plasma electron" component in addition to the streaming "beam electron" component. The unstable fluctuations of the two-stream instability may then begin to grow, at a rate which depends on the time-varying densities of beam and plasma electrons, and can reach amplitudes that lead to considerable heating of electrons, greatly enhanced electron-impact ionization of the remaining neutrals, and ultimately to thermal expansion of the heated source plasma.

On the other hand, at low pressures the ions created in the gas <u>are</u> removed axially from the gas region on the timescale of their creation. It is this component of ions, accelerated ahead out of the source plasma or gas into the beam-propagation region, that allows the beam front to move forward at the ion speed. If <u>all</u> the newborn ions were extracted at the rate they are produced, the ion density in the gas puff would not build up to $n_i = n_b$, and loss of IFR behavior would not occur. The instability in this case would be weak or nonexistent, and there is the possibility that a plasma object of beam electrons and extracted ions might have a reasonably low transverse temperature.

For this reason it is important to investigate the ion creation and extraction rates to try to define the regions of parameter space (gas pressure, beam current density, etc.) over which these two qualitatively different sorts of behavior (IFR and two-stream heating) will occur.

One useful hypothesis is that a quasi-steady state is reached, in which the ion extraction rate equals the creation rate. Since all newborn ions are accelerated in the quasi-static electric field of the beam, if we know the time-averaged potential drop over most of the gas region, and if we know that the beam head is advancing at a speed

$$v_h \sim \left(\frac{2\epsilon_b}{m_i}\right)^{1/2} \tag{22}$$

(with ϵ_b the beam-electron kinetic energy on entry to the gas), then we can use the continuity equation with an ionization source term to estimate the resident ion density in the gas puff, for quasi-steady conditions:

$$dn_i/dz \approx \nu_i(z)/\bar{v}_i(z) - n_i\dot{v}_i/v_i^2 \tag{23}$$

with $\nu_i(z)$ the local ionization rate (net rate if recombination is important) and $\dot{v}_i(z)$ the electric acceleration. (Here we used $\nabla \cdot v \approx \dot{v}/v$.) Simply put, if the volume $A_b v_h t$ ahead of the gas is filled with ions to a density $n_i \approx n_b$ (A_b is the transverse area of the beam), then quasi-steady conditions occur when the spatial integral, over the gas cloud, of $\nu_i(z)n_0(z)$, is equal to the ion flux, $n_b v_h$:

$$< \nu_i(z)n_0(z) >_z \ell_s \approx n_b v_h. \tag{24}$$

For a uniform gas density n_0 over a gas cloud of length ℓ_s then, the average ionization rate required for such quasi-steady conditions is

$$\bar{\nu}_i \approx \left(\frac{n_b}{n_0}\right)\left(\frac{2\epsilon_b}{m_i}\right)^{1/2} \ell_s^{-1} \tag{25}$$

If the ionization is predominantly done by ions being accelerated in the E_z field, as is the case in the code, we may estimate, for a given $E_z(z)$ profile and quasi-static ion flows,

$$\int_0^{\ell_s} dz \nu_i(v_i(z, z_1)),$$

with $v_i(z, z_1) = [2e(\phi(z_1) - \phi(z))/m_i]^{1/2}$, $\phi(z) \equiv -\int_0^z E_z(z')dz'$, and z_1, the birthplace of an ion, as a parameter. Using the approximate solution for $\nu_i(z)$ developed above for hydrogen (eq. 21), and neglecting ionization created in the thin "virtual cathode" sheath at $z \approx \ell_s$, we have an approximate condition for steady-state conditions at low pressure:

$$5.34(P/e_1)\left\{5.62(\ell_s e_1)^{0.2} - 1\right\} = \frac{k}{\ell_s P} - 1, \tag{26}$$

where $e_1 = E_1/(0.2\text{MV/cm})$, ℓ_s is in cm, P is in Torr, and

$$k \equiv \frac{1}{\beta c}\left(\frac{2\epsilon_b}{m_i}\right)^{1/2}\left[7.07 \times 10^{16}\ \sigma_{ebi}(\beta c)\right]^{-1} \tag{27}$$

with $\sigma_{ebi}(\beta c)$ the cross-section for ionization by beam electrons moving at speed βc. Eq. (26) is a condition relating the gas cloud width ℓ_s, the typical electric field strength $E_1 = (0.2\text{MV/cm})e_1$, and the pressure P, required for quasi-steady conditions (when P is low enough). The electron beam current has cancelled out from the expression because both the ionization rate and the downstream ion density are proportional to it, if photoionization is absent.

If the typical E-field value in the gas is taken from computer simulation, then at low pressures the conditions necessary for quasi-static behavior can be calculated and compared with the simulation for consistency.

Ion densities much higher than this should lead to avalanche and nearly complete ionization of the gas. Ion densities there much below this value could remain quasi-static (extraction balancing production), but would limit the density of the propagating electron + ion beam finger to the density available from ion extraction, i.e., the full density n_b of the electron beam source would not be found in the propagating plasma.

For beam energies $\epsilon_b \sim 1$ MeV, k in Eq. (27) is large enough that Eq. (26) simplifies to

$$P(Torr) \sim 0.4\left\{\frac{ke_1/\ell_s}{[5.6(\ell_s e_1)^{0.2} - 1]}\right\}^{1/2} \tag{28}$$

for the hypothetical steady situation. For expected values of e_1, this would give values of P on the order of 1 Torr. In fact, the low-pressure approximation is probably inaccurate above about 0.1 Torr (and thus the denominator expression in Eq. (28) is not to be taken very seriously), but the order-of-magnitude of P is probably still near 1 Torr, unless significant photoionization is present.

3 Source Plasma Heating – Theory

Once the plasma ion density is equal to the electron beam density (assuming ions are not expelled fast enough to prevent this), the main collisionless interaction of the electron beam with the ionizing gas puff is the two-stream instability. This instability transfers energy from

the beam in the form of nearly longitudinal (electrostatic) waves, and simultaneously acts through the wave-beam interaction to broaden the beam in momentum space as it advances through the plasma region.

If the electron beam and background plasma are relatively cold (i.e., the momentum spread of the beam is small), then the energy density in unstable electrostatic oscillations build up to a peak value of order

$$\epsilon_w = \gamma n_b \alpha \, mc^2 \frac{S}{2}(1+S)^{-5/2}, \quad S < \frac{1}{2} \ \text{(cold beam)} \tag{29}$$

where α is a numerical factor of order unity, and

$$S = \beta^2 \gamma (n_b/2n_p)^{1/3}, \tag{30}$$

before being limited by nonlinear processes (Thode and Sudan, ref. 7). This buildup of wave energy occurs on a timescale of several e-foldings of the instability. The inverse of the e-folding time is approximately

$$\Gamma_1 = Im\omega \approx \frac{3^{1/2}}{2\gamma}\left(\frac{n_b}{2n_p}\right)^{1/3} \omega_p \tag{31}$$

for a cold beam (hydrodynamic regime of instability). If the relativistic electron beam is warm or sufficiently scattered in pitch-angle (kinetic regime of instability), the growth rate is (Ref. 6)

$$\Gamma_1 = Im\omega \approx \frac{n_b}{\gamma n_p} \frac{1}{(\Delta\theta)^2}, \tag{32}$$

where $\Delta\theta$ is the angular width of the beam momenta.

Ordinarily, this growth is then limited or reversed after saturation by nonlinear effects other than trapping of beam electrons. On the time scale of ion motion across a few Debye lengths, high electric field regions (spikes) are formed which tend to exclude plasma ions and electrons by ponderomotive pressure (Refs. 8-11). This leads to the production of localized density reductions (cavitons). As these spikes sharpen and collapse (Ref. 8), their Fourier spectrum is broadened. By this means, the wave spectrum can change nonlinearly from waves with nearly a single wave vector to a spectrum that includes oscillation of zero phase velocity and waves in resonance with the tails of the plasma electron distribution. This

process, also an unstable one (Refs. 9-11) is referred to as the oscillating two-stream (OTS) instability.

There is a threshold energy for the onset of the OTS instability (Ref. 9). This threshold is reached when ϵ_1, the wave energy density in the unstable waves generated by the two-stream instability, becomes sufficiently large that the condition $\epsilon_1/nT \gtrsim (k_1\lambda_D)^2$ is satisfied, where $\lambda_D = (T/4\pi ne^2)^{1/2}$ is the Debye length and k_1 is the most unstable wave vector associated with the two-stream instability. For the case of a cold beam, Freund et al. (Ref. 11) find the growth rate to be

$$\Gamma^{\rm OTS} = \omega_p \epsilon_1/(4\pi nT) \tag{33}$$

when $3(k_1\lambda_D)^2 < \epsilon_1/nT < m/m_i$, and

$$\Gamma^{\rm OTS} = \omega_p \left(\frac{1}{3}\frac{m}{m_i}\frac{\epsilon_1}{nT}\right)^{1/2} \tag{34}$$

when $\epsilon_1/nT > m/m_i$ and $3(k_1\lambda_D)^2$.

After the threshold value of ϵ_1 is reached, the OTS instability begins feeding energy to plasma electrons on the timescale $2/\Gamma^{\rm OTS}$, as a result of stochastic acceleration of electrons crossing the cavitons. Energy is also fed into electromagnetic waves with $\omega \geq \omega_p$ (Ref. 12) and to ions (Refs. 16-18). Because new beam is continuously supplied to the region throughout the beam pulse, power is continuously supplied at a rate estimated to be

$$P({\rm erg/cm^3/s}) \sim 0.4 \times 10^{15} \left(\frac{n_b}{10^{12}{\rm cm^{-3}}}\right)^{5/3} \left(\frac{n_e}{10^{15}{\rm cm^{-3}}}\right)^{-2/3} (1+S)^{-5/2} \tag{35}$$

Some significant fraction ($\sim 1/2$) of this power goes into heating of plasma electrons, which subsequently lose energy by inelastic collisions, by expansion (Refs. 19-22), or by loss from the system. The energy input rate per plasma electron corresponds to a "heating rate"

$$\dot{T}_e + \frac{\dot{n}_e}{n_e}(T_e + 2\epsilon_i/3) \approx 170 f (1+S)^{-5/2} (10^3 n_b/n_e)^{5/3} \ \ {\rm eV/ns}, \tag{36}$$

where f is the fraction of deposited power delivered to electrons, and ϵ_i is the ionization energy per atom. Cooling by electron loss at their thermal speed, by comparison, occurs at a rate

$$\dot{T}_e({\rm eV/ns}) \sim 1330[T_e({\rm keV})]^{3/2} \ell_p^{-1}, \tag{37}$$

for a plasma of effective size ℓ_p (cm). And classical electron heat conduction could lead to a cooling rate

$$\dot{T}_e(\mathrm{eV/ns}) \sim -380[T_e(\mathrm{keV})]^{7/2}\ell_T^{-2}, \tag{38}$$

with an effective temperature gradient scalelength ℓ_T (cm), if the diode or surrounding gas serves as a heat sink.

For 1-centimeter scalelengths, then, one might expect mean electron thermal energies roughly of the order of seven hundred eV in the source plasma, with possible nonthermal 'tails' on the electron energy distribution there extending out to many keV. Once n_i exceeds n_b, a 10 ns beam-rise represents a few thousand plasma oscillation periods (their variation included), or several hundred growth times, and one may thus expect a fully-developed two-stream instability in the source plasma unless gradients, quasi-static electric fields, or other effects significantly damp the instability. (The plasma is only about 20 wavelengths thick, at the most unstable wavelength.)

Such a microinstability probably has three important effects besides generation of microwave diagnostic radiation: it can significantly heat the plasma, leading to rapid electron avalanche, it can make the plasma electrons effectively more collisional and less tied to magnetic field lines in laboratory experiments, and it can spread the energy distribution of the beam electrons. The first and last are, in fact, observed in the simulations described in the next section.

Some stabilizing influences which could reduce the plasma heating due to this microinstability have been studied. They are:

(a) electromagnetic effects, which can lead to a threshold current density for onset of the instability growth (Refs. 23-25);

(b) radial and longitudinal boundary conditions (Refs. 24-27);

(c) axial density gradient in the source plasma (Refs. 28-35);

(d) virtual-cathode-related electric field effects on instability growth (Refs. 36, 37);

(e) electron reflexing from a more realistic (non 1-D) beam head.

3.1 Threshold currents

These thresholds (Ref. 23) were found to be much lower than the currents of our simulations and the University of Maryland experiments. Instability growth should thus be unaffected.

3.2 Radial and longitudinal boundary conditions

The effects of radial boundaries were considered in Refs. (24) and (25). In anticipated experiments, the beam and pipe were large enough to contain several wavelengths of the most unstable wave. Stabilization by finite-radius effects is thus not expected.

Longitudinal boundary effects, including wave reflection, can have much more impact (Refs. 26, 27).

3.3 Axial finite-length effects and ion-density-gradient effects on two-stream growth

Using calculations of the spatial exponentiation length of the two-stream instability published by Rowland (Ref. 26), we find the growth length in a uniform-density plasma with $n_i > n_b$ to be

$$\ell_\gamma \text{ (cm)} \sim 0.5 \times 10^{-2} T_{eV}^{1/3} (\gamma - 1)^{1/6} \left(\frac{10^{15} \text{ cm}^{-3}}{n_{pe}} \right)^{1/6} \left(\frac{10^{12} \text{ cm}^{-3}}{n_b} \right)^{1/3} . \tag{39}$$

Thus, even as the plasma electrons become heated to ~10 keV, a 1 cm-long plasma source region always provides 20 or more growth lengths of the instability at $n_p = 10^{15}$ cm^{-3}, $n_b = 10^{13}$ cm^{-3}, $\gamma = 2$, provided n_p is uniform.

Next, from the work of Schmidt (Ref. 28), we have an estimate of the maximum number of e-foldings (of the unstable fields) allowed by any given density gradient in n_{pe}:

$$\mathcal{N} = 0.8 \times 10^3 h \left(\frac{n_{pe}}{10^{15} \text{ cm}^{-3}} \right)^{5/6} \left(\frac{n_b}{10^{12} \text{ cm}^{-3}} \right)^{2/3} \tag{40}$$

(for the non-collisional cold-beam instability), where h is the density gradient scaleheight,

$$h^{-1} = n_{pe}^{-1} |\partial n_{pe} / \partial z|. \tag{41}$$

The weak dependence of Eq. (38) on γ has not been included here because the theory is nonrelativistic. For anticipated parameters as above, then, nonlinear effects, rather than density gradients, would limit the e-folding if the beam is cold.

3.4 Effect of axial electric field on instability growth

When the residual quasi-static field in the plasma is of the order of the beam-electron trapping field E_T and is in the direction to retard beam electrons, a significant damping of the instability can occur (Refs. 36, 37).

3.5 Qualitative effect of radial beam electron loss instead of axial reflexing

In the code of section 4, which describes purely axial motion of beam and plasma electrons as if they were fully magnetized and did not transfer energy to perpendicular motion or temperature, beam electrons reaching the "beam head", i.e. the advancing ion front, reflex axially back toward the source (except for a few, which may leak forward and contribute the limiting current propagating in the vacuum). However, in a not-strongly-magnetized real situation, most of those beam electrons reaching the front would be lost radially – some sooner, some later – rather than specularly reflected from the front axially back to the source. Thus, code physics dependent on the presence of the counterstreaming reflected beam electrons is probably not to be taken as representative of real experimental conditions. Such physics includes heating of the propagating plasma/beam by two-stream-unstable waves arising from the beam-electron counterstreaming. It also includes a factor of two in the propagating region electron density and in the beam-electron density in the gas/source region.

Radial loss of beam electrons at the head of the propagating plasma also may alter the depth of the beam potential well there, because of the negative space charge.

4 Propagating Plasma Jet Formation – Theory

It appears that ions can be accelerated from the plasma by the motion of the steep potential gradient at the virtual cathode and, when applicable, by the unstable electrostatic waves brought to large amplitudes by streaming instability of the beam with the source plasma electrons (Refs. 16-18). These accelerated ions propagating into the low density background, together with the (reflexing) electrons of the beam, can form a low-density, partially neutralized plasmoid, which has an axial extent determined by the beam pulse duration, the

acceleration time, and the accelerated ion velocity,

$$\ell_p \sim (\tau_{eb} - \tau_a) v_i. \tag{42}$$

The density of this plasmoid is $\leq n_{eb}$, the accumulated density of reflexing beam electrons.

Another mechanism, qualitatively different, also produces a propagating dense plasma when the source plasma is sufficiently long in the axial direction: the unstable waves not only accelerate a few ions to quite high velocities ($v_{fi} \sim \beta c$) but also can heat a much larger fraction of source plasma electrons, which causes the source plasma to expand (the hot electrons electrostatically drag the plasma ions), and this thermal expansion, somewhat contained in other directions, forms a plasma jet in the beam direction which can have density $n_p \gg n_{eb}$ but has expansion front speed $v_f \sim M c_s \ll \beta c$ (M = Mach number, c_s = sound speed based on heated source-plasma electron temperature — "tail" temperature if appropriate.)

This plasma jet also forms a propagating plasmoid, terminating its ejection from the source plasma when the latter either cools or is exhausted. The cooling and evacuation of the source plasma may both be related to the instability heating in a complex nonlinear way: the instability growth should be altered by source-plasma density gradients, and the plasma heat source is the thermalizing of energy from the unstable waves. For the warm beam case (which our one-dimensional computer simulations indicate applies after a few ns) the coupled instability and hydrodynamics was treated in Refs. 19-22; the results are dependent on the plasma thermal conductivity and on the sensitivity of the Langmuir wave growth rate to the density gradients resulting from expansion (Refs. 23-31). The instability growth is also affected by the steep quasi-static potential gradient (Refs. 32,33) so that the two mechanisms are not completely independent.

Thus after a time lag it is possible that <u>two</u> plasma fronts will be seen advancing downstream: one for a fast, tenuous plasma ejected electrodynamically and one for a slower denser plasma ejected thermally. The timescale of our computer simulations is long enough to see the formation, if not the termination, of the faster one, but also shows the beginning of the thermally-produced one when the temperature reaches $\gtrsim 1$ keV. The energies in the fast and slow plasmoids can be estimated:

Fast: $n \sim n_{eb}$

$$\frac{1}{2}\ell_p n m_i V^2 \sim \frac{1}{2}(\tau_{eb} - \tau_a) n_{eb} m_i v_i^3, \tag{43}$$

Slow: $n \sim n_s \ell_s / \ell \sim n_s \ell_s / (c_s \tau_c)$

$$\frac{1}{2}\ell n m_i v^2 \lesssim \ell_s \frac{1}{6} n_{eb} (n_{eb}/n_c)^{1/3} (\gamma^2 - 1) m_e c^2, \tag{44}$$

in 1D, where $v_i^2 \sim (m_e/m_i)\beta^2 c^2$, n_{eb} is the reflexing electron beam density, and it was assumed that the heated source plasma, with "initial" density n_s and length ℓ_s, receives only a fraction $(n_{eb}/n_s)^{1/3}(\gamma+1)$ of the beam kinetic energy density, 1/3 of this going into directed kinetic energy via thermal heating, and undergoes a free expansion (here one-dimensional) on timescale τ_s.

The $\lesssim$ (rather than $\sim$) refers to the fact that once the reflexing electron beam is "warm", the growth rate of unstable energy deposition drops and the saturation energy density is also reduced, so that less energy may be available as thermal to drive the ablation of the slow plasma jet.

Numerically it is reasonable to expect the fast low-density plasmoid to contain more energy than the slower denser one if $n \sim n_{eb} \ll n_s$ and $v_i \gtrsim 0.1$ c.

Fast:

$$U(J/\mathrm{cm}^2) \sim 14 \left(\frac{n_i}{10^{12}\mathrm{cm}^{-3}}\right) \left(\frac{\tau_b}{10\mathrm{ns}}\right) \left(\frac{v_i}{0.1\mathrm{c}}\right)^3 \tag{45}$$

Slow:

$$U(J/\mathrm{cm}^2) \lesssim 7.4 \times 10^{-3} \left(\frac{\gamma^2 - 1}{3}\right) \left(\frac{n_{eb}}{10^{12}\mathrm{cm}^{-3}}\right)^{4/3} (f_i P_{torr})^{1/3} \left(\frac{\ell_{dep}}{1\mathrm{cm}}\right), \tag{46}$$

with f_i the degree of ionization in the source plasma and ℓ_{dep} the length over with beam energy is (partly) deposited.

However, if the electron beam is made to deposit most of its energy in the source plasma rather than leaving only an energy density

$$E^2/8\pi \sim (\gamma + 1)(n_{eb}/n_s)^{1/3}(\gamma - 1) n_{eb} m_e c^2, \tag{47}$$

or if this wave energy density can be transformed rapidly enough into thermal energy by nonlinear or collisional process, an "anomalous intense driver" (Ref. 38) of a more energetic

denser plasma jet may develop with

$$U(J/\mathrm{cm}^2) \sim \frac{1}{2}(\gamma-1)n_b m_e c^3 \beta \tau_b \sim 100(\gamma-1)\left(\frac{n_b}{10^{13}\mathrm{cm}^{-3}}\right)\left(\frac{\tau_b}{10\mathrm{ns}}\right). \qquad (48)$$

(This may require a longer plasma.)

The relative merits of such a hot plasma jet, as compared with the tenuous but energetic electron and accelerated ion plasmoid, should now be considered. Specifically, we consider transverse temperature. Collectively accelerated ions can, in principle, have very little transverse temperature, but a plasma jet, even after expansion cooling, would be expected to have transverse beam-heated thermal energy comparable with its directed energy (Ref. 39). In the absence of an axial confining magnetic field, or of transverse cooling by some rapid means, radial expansion velocities would be only somewhat less than axial expansion velocity. For a 1 keV hydrogen plasma this would be of order 10^8 cm/s. Initially, at least, such a dense plasmoid would be quasi-neutral and have $J_i \approx |J_e|$ and so would not be constrained by magnetic self-focusing due to its own current. By contrast, the lower density plasmoid with accelerated ions need not be quasi-neutral, but would have electrostatic forces from its initial space charge imbalance and/or from the preferential scattering of one species (usually electrons) out of the co-moving plasma by collisions.

The radial forces on electrons and ions in a partially-neutralized long cylindrical beam (plasmoid) of "co-moving" electrons and ions can best be considered in the plasmoid frame, once this object is detached from its source and propagating in a tenuous background. This analysis, although the electrons may have relativistic "temperature" in this frame, transforms back to the laboratory frame rather simple because the relative velocity is less than about 0.1 c. In the plasmoid frame there is almost no axial net current (except possibly for fast oscillations with zero average, which should damp rapidly by phase mixing). For times short compared with electron isotropization, the transverse electron temperature could be assumed nonrelativistic as well, but the rapid growth of high-frequency fluctuations in the formation state (many with $k_\perp \neq 0$) indicates that a better assumption might be nearly-isotropic electrons with most of their initial directed energy now appearing as thermal energy in the plasmoid frame (Ref. 39). Ignoring the background ions, then, this long plasmoid expands radially under its pressure gradient and net space-charge forces. While at early times the

electron radial accelerations may significantly exceed those of the ions, in a few plasma periods the radial space-charge oscillations damp to an ambipolar one-fluid expansion at a few times the ion sound speed. Provided the electrons do not escape at early times enough to lower ω_{pe} below ω_{pi}, we may take the asymptotic time dependence of $\omega_{pe}(t)$ as controlling the damping of the radial space-charge pulsations.

For radial expansion at the sound speed $\sim (T_e/m_i)^{1/2}$, the ratio of radial to axial speeds in the laboratory frame is roughly

$$\frac{\dot{r}}{\dot{z}} \sim [(\gamma - \Delta\gamma - 1)m/m_i]^{1/2}\bar{\beta}_z^{-1}(r_0/r)^2, \tag{49}$$

where $\Delta\gamma$ is the energy loss in the formation and counterstreaming stages of early development, in units of mc^2; m without subscript refers to the electron rest mass, and adiabatic cooling ($T_e \propto r^{-2}$) has been assumed. For the experimental beams in our laboratory (and simulations), with $\gamma \approx 2$ and $\Delta\gamma \approx 0.1$, $m_i = 1836$ m, and $\bar{\beta}_z \sim 0.02$, this would give an initial expansion cone with initial half-angle of about 49° or larger, which is unacceptable for some applications, and is probably made worse by increasing γ.

Ignoring electrostatic assistance of the expansion, one derives

$$r(z) \sim r_0[1 + 3\kappa z\beta_z^{-1}r_0^{-1}]^{1/3}, \tag{50}$$

with

$$\kappa \sim [(\gamma - \Delta\gamma - 1)m/m_i]^{1/2}. \tag{51}$$

For the laboratory conditions above, this would lead to expansion from $r_0 = 0.5$ cm to $r \gtrsim 9$ cm in 1 m of travel at $\beta_z = .02$ (for protons).

The conclusion of this portion of the analysis, then, is that only by using higher-mass ions and/or preventing electron isotropization can the radial expansion rates in vacuum be kept low enough. It is unlikely that electron isotropization can be prevented, as it results from the electron reflection at the advancing plasmoid front as well as from unstable waves with radial components of k.

The low-density background plasma streaming through this plasmoid in its frame can affect the radial expansion if its electrons are slowed more than its ions (generating a net current and thus an aximuthal magnetic field in the plasmoid frame); the magnetic effect is

slight if the magnetic energy density is small compared with the thermal energy density of the isotropized plasmoid electrons. This is generally the case until the plasmoid radius is quite large

$$\frac{B^2}{8\pi} \lesssim \frac{\pi}{2} e^2 r^2 [\Delta(n_b\beta)]^2 \tag{52}$$

where $\Delta(n_b\beta)$ is the value of $n_{bi}\beta_i - n_{be}\beta_e$ in the background (in the plasmoid frame) caused by effective "collisions" with the denser plasmoid, and r is the radial extent of the plasmoid. Thus,

$$\begin{aligned} \frac{n_p T_p}{B^2/8\pi} &\sim \frac{2n_p}{\pi r^2 e^2} \frac{(\gamma - \Delta\gamma - 1)mc^2}{[\Delta(n_b\beta)]^2} \frac{r_0^2}{r^2} \\ &\sim 8\left[\left(\frac{r_0}{r}\right)\left(\frac{n_p}{\Delta n_b\beta}\right)\left(\frac{c}{r\omega_p}\right)\right]^2 (\gamma - \Delta\gamma - 1). \end{aligned} \tag{53}$$

Here c/ω_p is the collisionless plasmoid skin depth, and we have allowed the plasmoid to cool by adiabatic expansion from its creation radius r_0. Taking the plasmoid density reduction (from radial expansion) into account, the magnetic effects are important only once

$$r \gtrsim 2.8\left(\frac{c}{\omega_{p0}}\right)\left[\frac{\Delta(n_b\beta)}{n_p}\right]^{-1} (\gamma - \Delta\gamma - 1)^{1/2}, \tag{54}$$

where $\Delta(n_b\beta)/n_p$ is approximately constant, and where the skin depth at injection is

$$\frac{c}{\omega_{p0}} = .173\left(\frac{10^{13}}{n_{p0}}\right)^{1/2} (\text{cm}). \tag{55}$$

Since n_p/n_b is quite large (n_b here is the background electron density in the "vacuum" region), magnetic braking of the plasmoid expansion should occur only for large plasmoid radius, if then.

If background electrons are scattered into a halo surrounding the plasmoid (leaving the background ions in the plasmoid), there is a slight electrostatic inward tracking force which partially offsets any electrostatic outward force on plasmoid electrons due to their own charge excess (i.e., $n_{ep} - n_{ip} > 0$).

5 1D Simulation of Source Plasma and Plasma Jet Formation

[Basic PIC code and results are published, *J. Appl. Phys.* **67**, 1650 (1990). A copy is attached.]

5.1 Beam Cutoff Studies

To investigate the possibility of forming a charge- and current-neutral plasmoid in our system, we modified the PIC code which we have been using to simulate plasma-jet formation so that the electron beam cuts off in the middle of a run. Results are shown for one such run in which a 500-kV, 15-kA, 5-mm-radius electron beam is injected into a 4-cm-radius, 40-cm-long drift tube with a 600-mTorr, 1-cm-wide cloud of hydrogen gas located next to the anode plane.

In Figure 1, the density profile for each particle species and the net charge density profile are shown at intervals of 2000 time steps (which corresponds to about 1.5 ns of real time) after the beam has been turned off. Before the beam is turned off, a plasma jet, composed of beam electrons and plasma ions with nearly equal densities of approximately 10^{12} cm^{-3} extends from the end of the source plasma to a distance approximately 20 cm downstream. (The source plasma can be identified by the large spike in the plasma ion density profile.) After the beam is turned off, the tail of the plasma jet detaches from the source plasma, forming a plasmoid composed of plasma ions and beam electrons. After detaching from the source plasma, the plasmoid continues downstream at a velocity of between 0.04c and 0.05c.

As time progresses, the number of particles in the source plasma continues to increase, even though the electron beam has been turned off. At the same time, the source plasma begins to expand downstream. Unfortunately, the combination of these two effects makes simulation of the plasmoid difficult at later times. Because of computer limitations, the code halves the number of macroparticles in the simulation whenever the number becomes too large. As the number of particles in the source plasma increases, the number of macroparticles in the plasmoid is therefore constantly being reduced. Also, as the source plasma expands outward, it overtakes the plasmoid and the plasmoid is no longer distinguishable from the source plasma.

Figure 2 shows the density profile for each particle species for a run in which the source plasma was artificially removed after the plasmoid had detached itself from the source plasma. The density profiles are shown 20,000 time steps (15 ns) after the beam was turned off.

5.2 Pressure Variation Studies

We have performed a number of simulations with different neutral gas pressures. Qualitatively, we were able to identify four pressure regimes - ultra-low, low, intermediate, and high.

In the ultra-low-pressure regime, the neutral-gas pressure is too low to produce a significant amount of ionization during the simulation. No significant movement of the virtual cathode is observed, the electron current which is measured downstream equals the value of the space-charge limiting current for the system, and no ions are detected downstream.

In the low-pressure regime, sufficient ionization is produced to cause motion of the virtual cathode downstream through the gas cloud. As the virtual cathode moves through the gas, ions from the ionized gas are accelerated to energies several times the electron beam energy. The potential in the region behind the virtual cathode also becomes positive. The gas pressure is too low, however, to maintain the forward position of the virtual cathode, and the virtual cathode quickly returns to its original position near the anode plane. The electron current measured downstream slightly exceeds the space-charge limiting value, and a weak ion current is detected downstream.

In the intermediate-pressure regime, the gas pressure is sufficiently high that the virtual cathode is able to maintain its position after reaching the end of the gas cloud, and a quasi-steady state is achieved. In the steady state, ions are created at a rate which just balances the rate at which they are extracted from the source plasma by the electric fields of the virtual cathode, which is located just downstream of the source plasma, and the rate at which they are ejected from the source plasma through the anode plane by the positive potential in the source plasma. The plasma electrons are also ejected from the source plasma through the anode plane by a mechanism which we have not yet identified. The majority of beam electrons continue to be reflected back through the anode plane by the virtual cathode. However, a significant fraction travel past the virtual cathode and down the drift tube until they reach the head of the beam of ions which have been extracted from the plasma by the virtual cathode fields. Most of the electrons are reflected at the head of the beam of ions but some continue downstream, creating a current equal to the space-charge limiting current.

In Figure 3, we show the electron and ion momentum distributions at a point in the

plasma jet downstream from the source plasma but upstream from the head of the jet for one run in the intermediate pressure regime.

In the high-pressure regime, the gas pressure is too high to maintain a quasi-steady state. The number of ions and electrons in the source plasma increases with time, and the electron temperature in the source plasma also increases with time. At a certain time, the plasma electrons become sufficiently energetic that they suddenly jet downstream, dragging the ions in the source plasma downstream with them.

6 Momentum and Energy Exchange Between a Dense Propagating "Plasmoid" and a Tenuous Background Plasma

We have analyzed here to a limited extent both collisional and electrodynamic processes. Under almost all circumstances the latter dominate when the background is tenuous. The collision processes examined included large-angle scattering and charge exchange (for weakly-ionized hydrogen background) between plasmoid particles and background particles. More significant are the effects on the energy and momentum exchange mediated by a level of fluctuations enhanced above the thermal level and mediated by the non-neutrality of the plasmoid when its net charge density exceeds the background plasma density.

Electron scattering within the dense plasmoid, in its own frame, continually repopulates the electron Maxwell tail above the electrostatic potential-well depth, allowing electrons to escape. The potential well depth adjusts so that the ion expulsion rate due to the potential equals the electron loss rate. When Coulomb collisions dominate the scattering loss, this ambipolar potential, neglecting the background, is $e\phi/T_e \sim \frac{1}{2}\ell n\sqrt{m_e/m_i}$, occurring over the density gradient scalelength of the dense plasma (roughly half its dimension).

The effects of the low density streaming background are (if $\phi > 0$):

(a) Background electrons ahead of the plasmoid are radially attracted, weakly magnetized by their net current ($\sim en_b\Delta v_{ez}$), and axially slowed temporarily, thus increasing their density locally. If $n_{pi} - n_{pe}$ is larger than the resulting $n_{eb} - n_{ib}$, this is of little consequence for plasmoid electrons.

(b) In the frame of the dense plasma, the flowing low-density background plasma contains

a (quasi-static?) nonneutral downstream wake. While background ions are too heavy to have their motion strongly perturbed, for a positively-charged plasmoid the background electrons are accelerated radially into and out of the plasmoid, being temporarily 'heated' in the process. These accelerations can occur on the electron inertial timescale, i.e., ω_{pb}^{-1}, thus establishing a plasma space-charge oscillation (or standing-wave perturbation) which is the large-amplitude version of the perturbation of background plasma by a test charge. Here the 'test charge' has finite extent and $e\phi \gtrsim T_{eb}$, so the space-charge perturbation in the wake can have $\delta n_e/n_{eb} \sim 1$ and $e\phi \sim T_{pe}$ over a radial scalelength comparable to the dense-plasma radius.

(c) By enhancing the electric field fluctuation level in the plasmoid, the streaming background enhances the effective energy-exchange collision rate of the dense electrons above the Coulomb value ν_e; thus the energy tail of the electron distribution function would be populated faster, assuming $\beta c > 2v_{th}$ in the plasmoid. In order to compensate for the increased escape of electrons over the electrostatic barrier, the plasma potential must be increased to allow both ions and electrons to be lost at equal rates. The potential increases by an additive $\ell n(\nu_L^*/\nu_L)$, where ν_L is the electron loss rate in the absence of enhanced fluctuations and ν_L^* is the enhanced loss rate. In steady state, ν_L is proportional to ν_e. Once $\nu_e^* \gg \nu_e$ the potential change should scale with the logarithm of the fluctuation level, and the energy invested in quasi-static potential is proportionately larger. The fields are thus larger for given plasmoid size, when $\beta c \gg v_{th}$, but the energy dissipation rates are not strongly affected by these electrostatic fields.

However, the fluctuations, supplied by background streaming energy (i.e., in the lab frame by plasmoid slowing), also serve to heat the plasmoid electrons until $\beta c \sim v_{th}$. Then the loss region ($e > e\phi$) is depopulated by trapping background electrons almost as fast as it is populated by tail-filling from the denser electrons (as one can see by looking at phase-space orbits near the trapped-untrapped boundary), and the plasma potential and associated quasi-static E-field decrease.

(d) The magnetic field in the plasmoid frame due to the change in v_z of the streaming background electrons slightly impedes the thermal expansion of the plasmoid in the radial direction, as discussed above.

7 Discussion and Conclusions

The injection of an intense electron beam into a localized gas cloud can lead to the acceleration of a 'plasma clump', with density comparable to the beam density, from the downstream side of the gas into vacuum, at a speed corresponding to beam electron energies and ion mass. This is the expected situation provided the degree of ionization in the gas remains low. Extraction of the ions by the axial electric field as they are produced at a low pressure helps maintain this $n_i < n_b$ situation, and rapid expulsion of newly-created electrons keeps $n_e \ll n_b$ in the gas while $n_i < n_b$ there. If the cathode is hot enough to emit ionizing radiation, the gas should be shielded (or shadowed) from it in order to avoid photoionization.

If, as at higher pressures, n_i builds up to exceed n_b, it is predicted that electron density comparable to n_b or greater can build up in the source gas, leading to rapid electron heating by two-stream instability, electron-impact avalanche of the remainder of the gas, and a thermal explosion producing a denser jet of plasma with much larger transverse (thermal) energies than in the case of strictly "electrostatic" acceleration. During the course of beam injection at pressures on the order of 1 Torr and above, both the fast tenuous directed jet and, subsequently, the slower, denser jet of the thermal explosion are predicted, and are seen in a 1D simulation. After beam turnoff, at low pressures a plasmoid with $n_i \sim n_b$ is seen in simulations to separate from the source gas and propagate downstream. At higher pressures, simulation shows this being followed, even overtaken, by a thermal-explosion jet in which plasma electrons have been very strongly heated.

The interaction of a propagating, expanding plasmoid with a very tenuous ionized background plasma has also been considered. Electrostatic effects are expected to dominate over collisional or magnetic effects. Enhanced electric field fluctuations in the propagating plasmoid are predicted to raise its transverse electron temperature and thus contribute to its reduction in axially-directed energy flux density due to enhanced radial expansion.

8 References

1. J. Guillory et al., "Annual Technical Report: Formation and Stability of Partially Neutralized Plasma Clumps, AFOSR, January, 1987.

2. G.R. Cook and P.H. Metzger, "Photoionization and Absorption Cross Section of H_2 and D_2 in the Vacuum Ultraviolet," J. Opt. Soc. Am. **54**, 568 (1964).

3. J. Poukey and C. Olson, "Charge-Neutralization Processes for Relativistic Electron Beams in Low-Presssure Neutral Gases," Phys. Rev. A **11**, 288 (1975).

4. B.B. Godfrey, W.R. Shanahan, and L.E. Thode, "Linear Theory of a Cold Relativistic Beam Propagating Along an External Magnetic Field," Phys. Fluids **18**, 346 (1975).

5. S.A. Bludman, K.M. Watson, and M.N. Rosenbluth, "Statistical Mechanics of Relativistic Streams," Phys. Fluids **3**, 747 (1960).

6. B. Breizman and D. Ryutov, Sov. Phys. JETP **33**, 220 (1960).

7. L.E. Thode and R.N. Sudan, Phys. Rev. Lett. **30**, 732 (1973).

8. V.E. Zakharov, Sov. Phys. JETP **35**, 908 (1972).

9. K. Papadopoulos, "Nonlinear Stabilization of Beam-Plasma Interactions by Parametric Effects," Phys. Fluids **18**, 1769 (1975).

10. H. Schamel, Y.C. Lee, and G.J. Morales, "Parametric Excitation of Ion Density Fluctuations in the Relativistic Beam-Plasma Interaction," Phys. Fluids **18**, 1769 (1975).

11. H.P. Freund, I. Haber, P. Palmadesso, and K. Papadopoulos, "Strongly Turbulent Stabilization of Electron Beam-Plasma Interactions," Phys. Fluids **23**, 518 (1980).

12. J. Dawson and C. Oberman, "High-Frequency Conductivity and the Emission and Absorption Coefficients of a Fully Ionized Plasma," Phys. Fluids **5**, 517 (1962); ibid. Phys. Fluids **6**, 394 (1963).

13. B. Smith, M. Goldstein, and K. Papadopoulos, Solar Phys. **46**, 515 (1976).

14. T.J.M. Boyd and J.J. Sanderson, *Plasma Dynamics* (Barnes and Noble, New York, 1969).

15. J.D. Jackson, J. Nucl. Energy (Part C) **1**, 171 (1960); ibid, *Classical Electrodynamics*, Second Edition (Wiley, New York, 1975).

16. K. Alexander et al., "A Simple Model for the Acceleration of Ions by High-Current Relativistic Electron Beams," Sov. Phys. JETP **40**, 280 (1974).

17. V.N. Tsytovich, "Relativistic Solitons and Nonlinear Waves as Bunches for Coherent Acceleration," Sov. Phys. Dokl. **7**, 31 (1969).

18. B.B. Godfrey and L.E. Thode, "Collective Ion Acceleration via the Two-Stream Instability," $[n_b \geq n_p]$ Los Alamos Tech. Report LA-UR 74-545, 1974.

19. A.T. Altyntsev et al., IAEA Conf. on Plasma Physics and CTR, Madison, 1971 (IAEA/CN-28) Paper E20.

20. G. Benford, "Radial Plasma Response During Intense Beam Heating," Phys. Rev. Lett. **39A**, 247 (1972).

21. J.D. Kilkenny, "Limitations on the Radial Acceleration of a Plasma Formed by an Intense Relativistic Electron Beam," Plasma Phys. **18**, 905 (1976).

22. K.R. Chu et al., "Ion Heating by Expansion of Beam-Heated Plasma," NRL Memo Report 3044, April 1975.

23. H.S. Uhm, "Electromagnetic Description of the Two-Stream Instability in a Relativistic Electron Beam," Naval Surface Weapons Center, Report NSWC MP84-236, May 1984.

24. P.F. Ottinger and J. Guillory, "Effects of Finite Radial Beam Geometry and Magnetic Self-Fields on Beam-Plasma Interactions in a Plasma-Filled Waveguide," Phys. Fluids **22**, 476 (1979).

25. W.L. Kruer and A.B. Langdon, "Electromagnetic Effects in Relativistic Electron Beam Plasma Interactions," Proc. 2nd Workshop on Laser Accel. of Particles, January 1985.

26. H.L. Rowland, "Convective Growth of the Two-Stream Instability," Phys. Fluids **B1**, 700 (1989).

27. I.G. Morey, and R.W. Boswell, "Evolution of Bounded Beam-Plasma Interaction in a One-Dimensional Particle Simulation," Phys. Fluids **B1**, 1502 (1989).

28. G. Schmidt, "Beam-Plasma Instability in a Nonuniform Plasma," Phys. Rev. Lett. **33**, 287 (1974).

29. W.R. Shanahan, "Multidimensional Theory of the Inhomogeneous Beam-Plasma Instability," Phys. Fluids **21**, 1808 (1978).

30. A. Reiman, "Space-Time Evolution of Nonlinear Three-Wave Interactions. II. Interaction in an Inhomogeneous Medium," Rev. Mod. Phys. **51**, 311 (1979).

31. B.N. Breizman and D.D. Ryutov, "Quasilinear Relaxation of an Electron Beam in an Inhomogeneous Bounded Plasma," Sov. Phys. JETP **30**, 759 (1970).

32. Yu. P. Bliokh, V.D. Shapiro, and V.I. Shevchenko, "Quasi-Linear Theory of Beam Heating in a Non-Uniform Plasma," Nucl. Fusion **12**, 301 (1972).

33. A.K. Berezin et al., "Influence of Longitudinal Density Gradient on the Transformation and Emission of Transverse Waves from a Beam-Plasma Discharge," Sov. Phys. JETP Lett. **14**, 97 (1971).

34. R.A. Demirkhanov et al., "Investigation of the Mechanism of Heating of the Plasma Electron Component under Two-Stream Instability Conditions in a Mirror Trap," Sov. Phys. JETP **36**, 874 (1973).

35. H. Böhmer, E.A. Jackson, and M. Raether, "Quenching of the Beam-Plasma Instability of Mode Mixing at a Density Discontinuity," Phys. Fluids **16**, 1064 (1973).

36. G.J. Morales, "Effect of a DC Electric Field on the Trapping Dynamics of a Cold Electron Beam," Phys. Fluids **23**, 2472 (1980).

37. S.I. Tsunoda and J.H. Malmberg, "Wave Enhancement Due to a Static Electric Field," Phys. Fluids **27**, 2557 (1984).

38. L.E. Thode, "Anomalous Intense Driver Experiment," Los Alamos National Laboratory Report, LA-7715-MS, March 1980.

39. D.A. Whelan and R.L. Stenzel, "Nonlinear Energy Flow in a Beam-Plasma System," Phys. Rev. Lett. **50**, 1133 (1983).

9 Figure Captions

Figure 1. Beam-electron, plasma-ion, and plasma-electron density profiles and net-charge-density profile at time steps (a) 20,000, (b) 22,000, (c) 24,000, and (d) 26,000. Number densities are shown in units of number cm^{-3}, charge densities are shown in units of C m^{-3}, and distances are measured from the anode plane in cm.

Figure 2. Beam-electron, plasma-ion, and plasma-electron density profiles and net-charge-density profile at time step 40,000 for a run in which the source plasma has been artificially removed.

Figure 3. Momentum distributions for (a) beam electrons and (b) plasma ions at 20 cm at 40,000 time steps for a run in the intermediate-pressure regime.

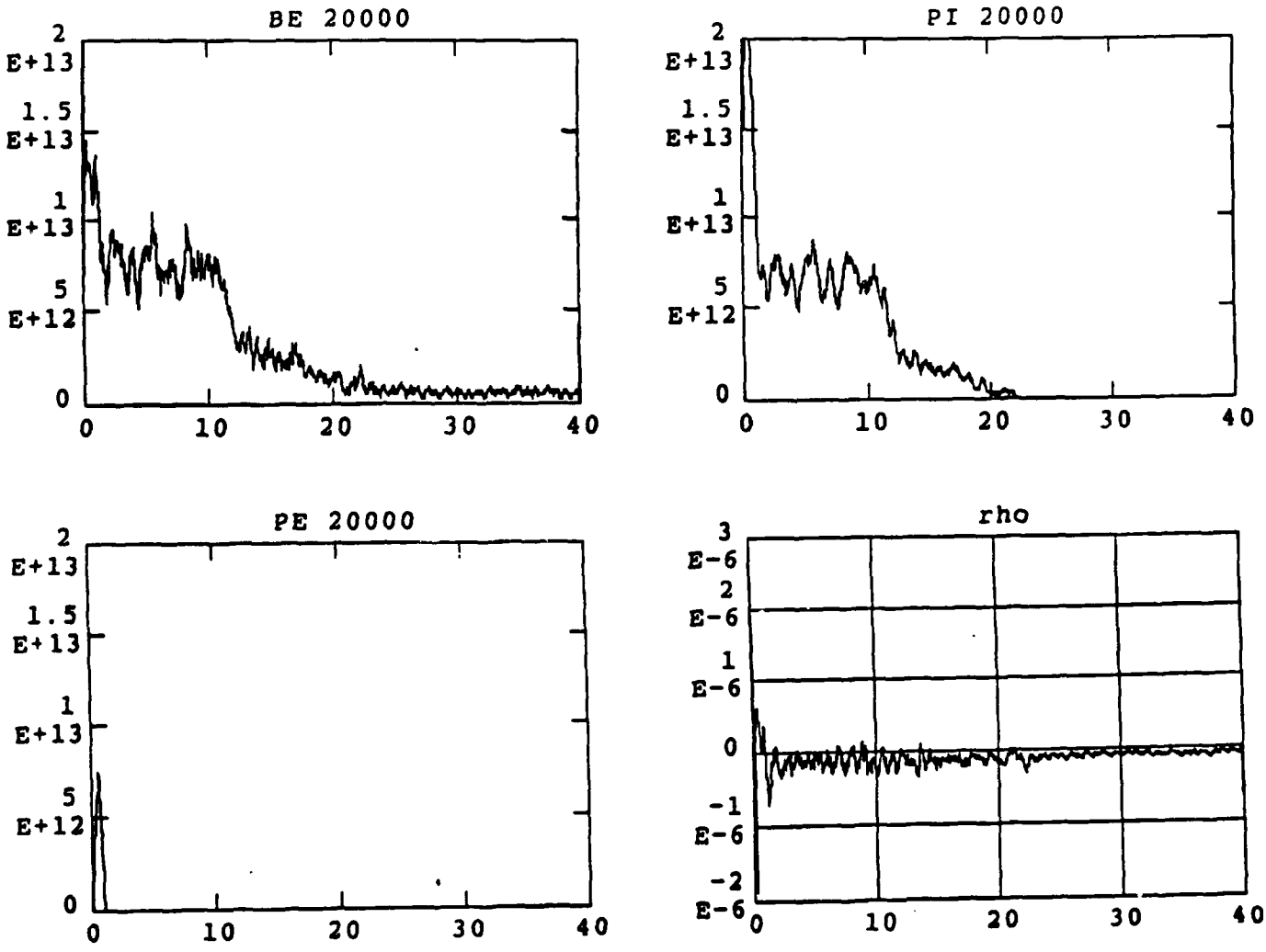
BE 20000
2 E+13
1.5 E+13
1 E+13
5 E+12
0
0 10 20 30 40
PI 20000
2 E+13
1.5 E+13
1 E+13
5 E+12
0
0 10 20 30 40
PE 20000
2 E+13
1.5 E+13
1 E+13
5 E+12
0
0 10 20 30 40
rho
3 E-6
2 E-6
1 E-6
0
-1 E-6
-2 E-6
0 10 20 30 40

FIG. 1a

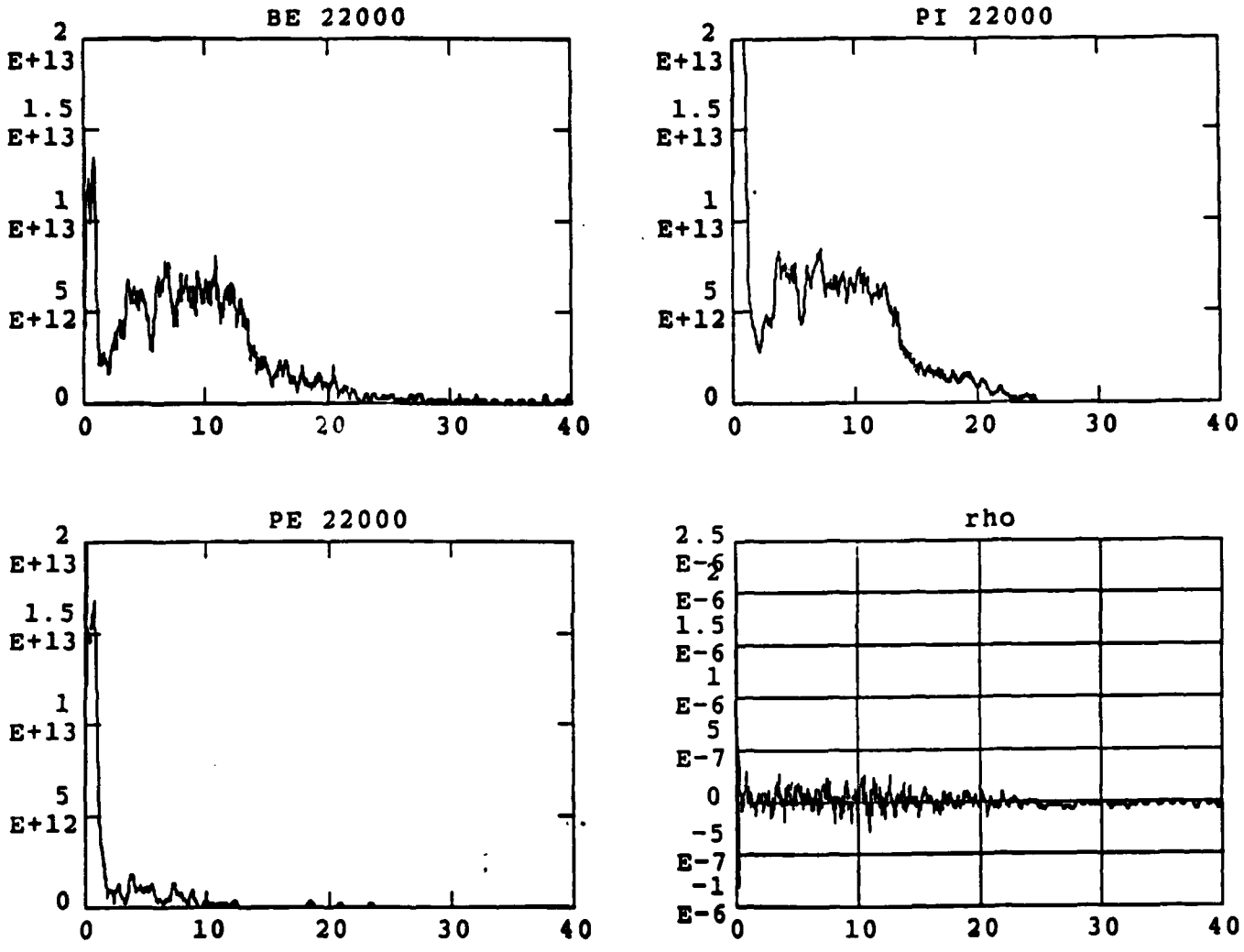
BE 22000
2 E+13
1.5 E+13
1 E+13
5 E+12
0
0 10 20 30 40
PI 22000
2 E+13
1.5 E+13
1 E+13
5 E+12
0
0 10 20 30 40
PE 22000
2 E+13
1.5 E+13
1 E+13
5 E+12
0
0 10 20 30 40
rho
2.5 E-6
2 E-6
1.5 E-6
1 E-6
5 E-7
0
-5 E-7
-1 E-6
0 10 20 30 40

FIG. 1b

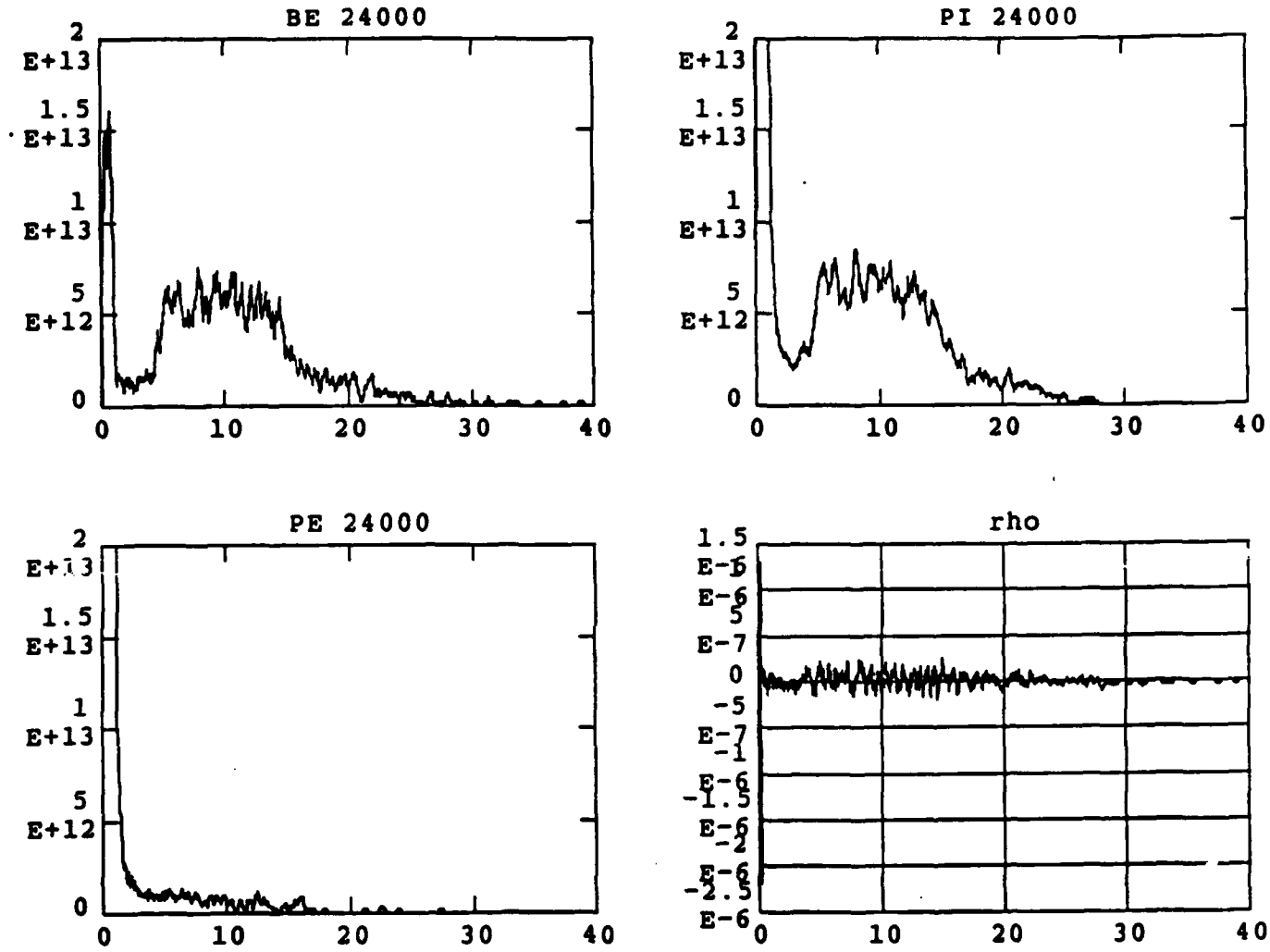
BE 24000
2 E+13
1.5 E+13
1 E+13
5 E+12
0
0 10 20 30 40
PI 24000
2 E+13
1.5 E+13
1 E+13
5 E+12
0
0 10 20 30 40
PE 24000
2 E+13
1.5 E+13
1 E+13
5 E+12
0
0 10 20 30 40
rho
1.5 E-6
5 E-7
0
-5 E-7
-1 E-6
-1.5 E-6
-2 E-6
-2.5 E-6
0 10 20 30 40

FIG. 1c

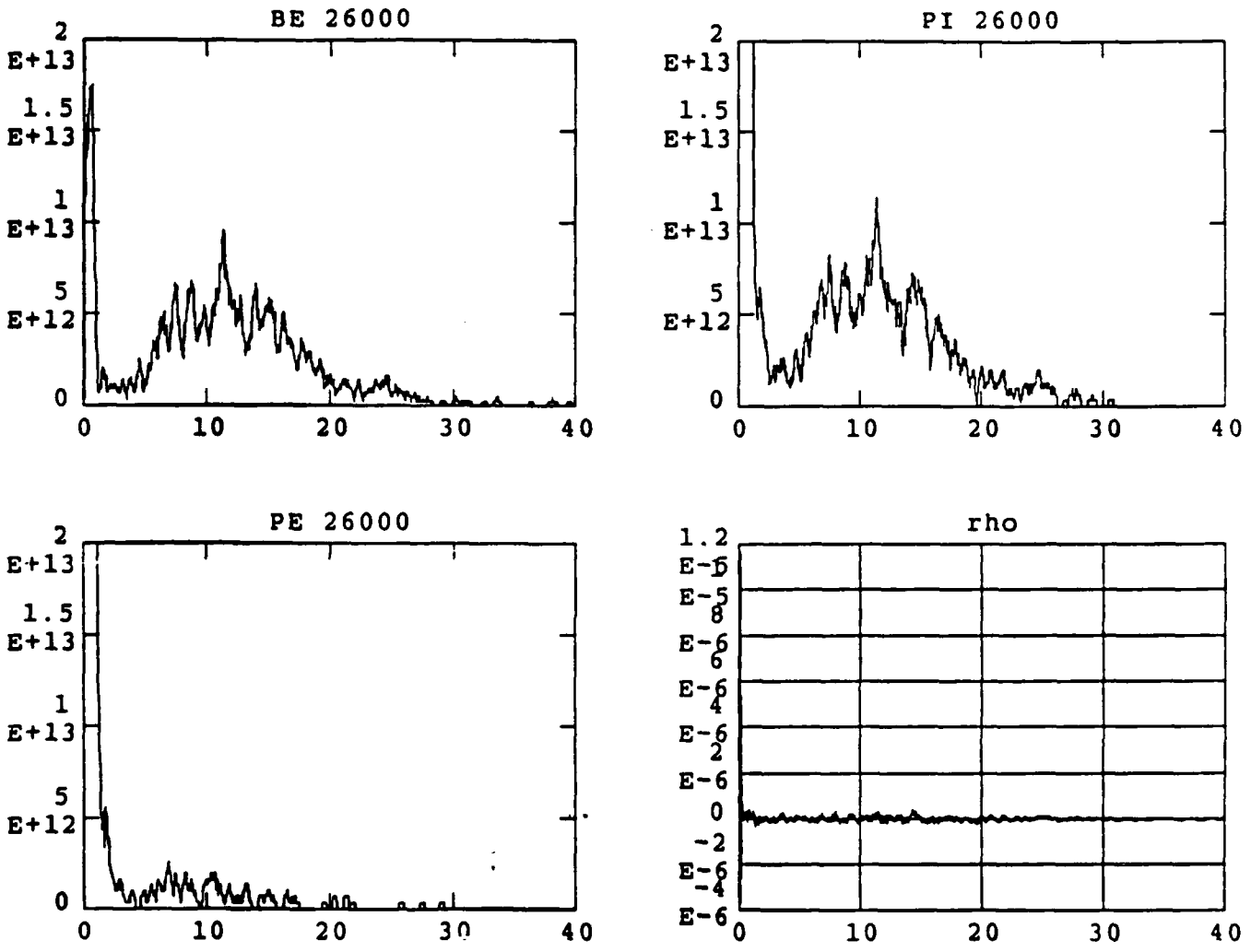
BE 26000
2 E+13
1.5 E+13
1 E+13
5 E+12
0
0 10 20 30 40
PI 26000
2 E+13
1.5 E+13
1 E+13
5 E+12
0
0 10 20 30 40
PE 26000
2 E+13
1.5 E+13
1 E+13
5 E+12
0
0 10 20 30 40
rho
1.2 E-5
1 E-5
8 E-6
6 E-6
4 E-6
2 E-6
0
-2 E-6
-4 E-6
0 10 20 30 40

FIG. 1d

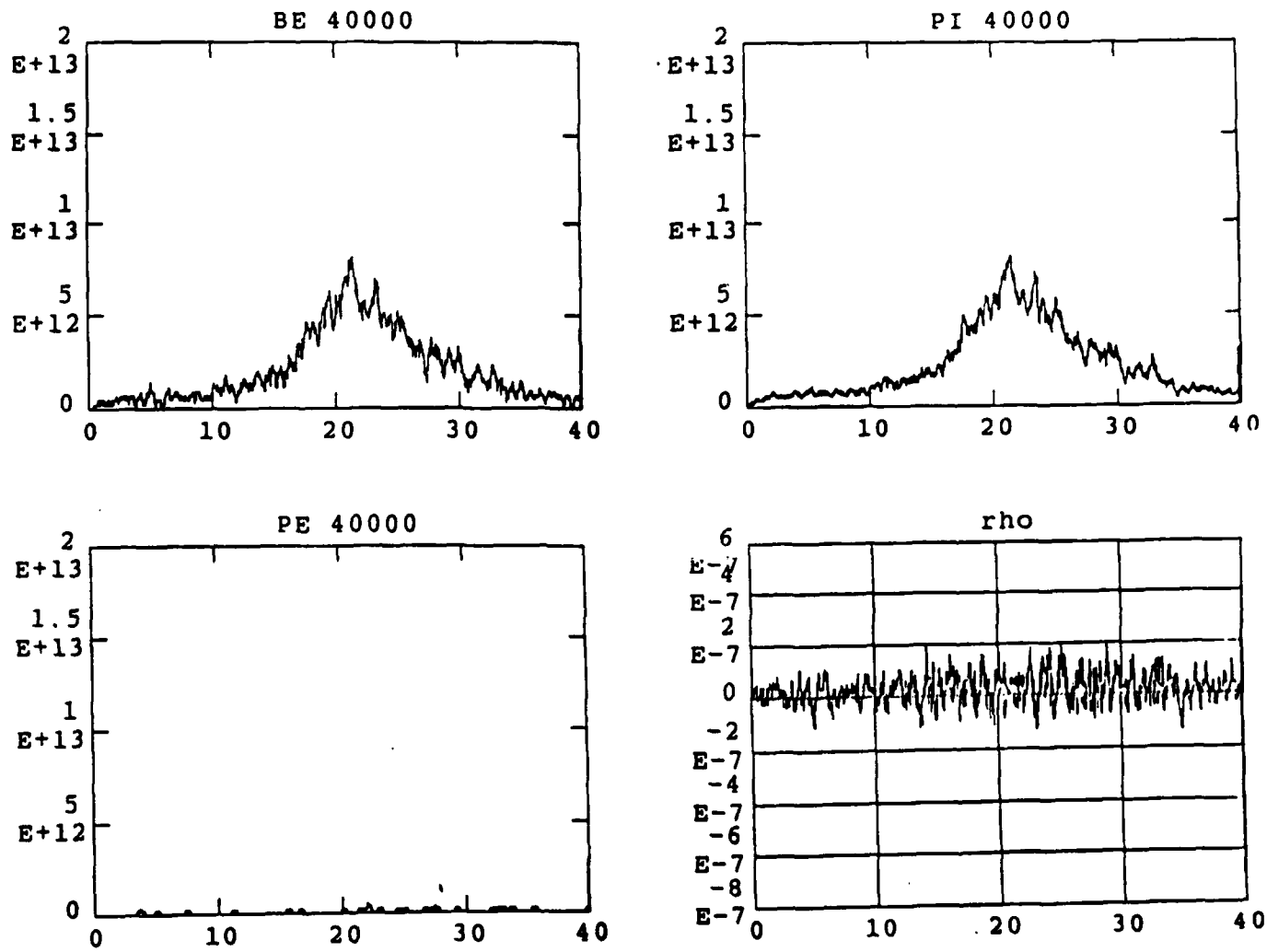
BE 40000
2 E+13
1.5 E+13
1 E+13
5 E+12
0
0 10 20 30 40
PI 40000
2 E+13
1.5 E+13
1 E+13
5 E+12
0
0 10 20 30 40
PE 40000
2 E+13
1.5 E+13
1 E+13
5 E+12
0
0 10 20 30 40
rho
6 E-7
4 E-7
2 E-7
0
-2 E-7
-4 E-7
-6 E-7
-8 E-7
0 10 20 30 40

FIG. 2

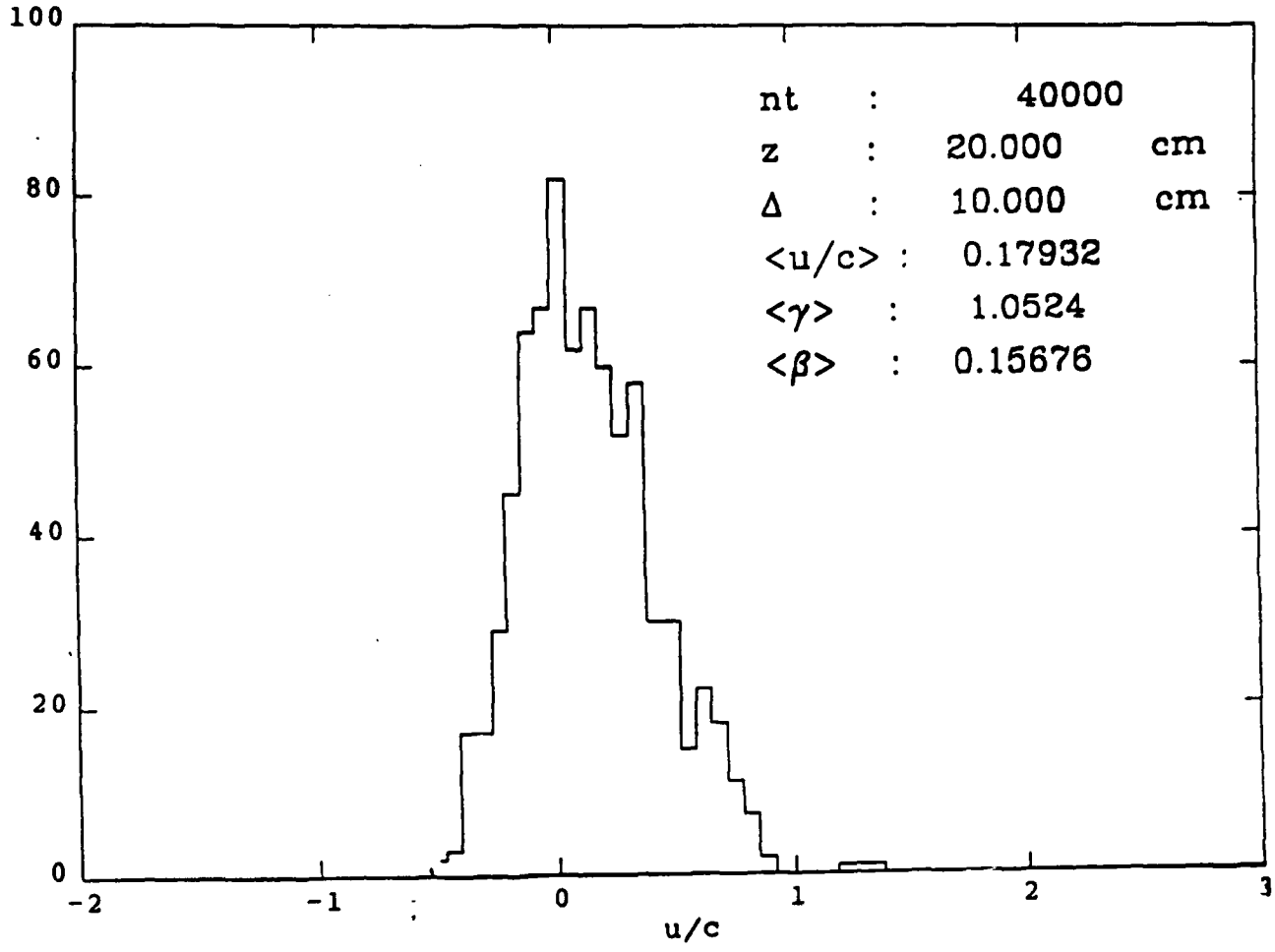
100
80
60
40
20
0
-2
-1
0
1
2
3
u/c
nt : 40000
z : 20.000 cm
Δ : 10.000 cm
<u/c> : 0.17932
<γ> : 1.0524
<β> : 0.15676

FIG. 3a

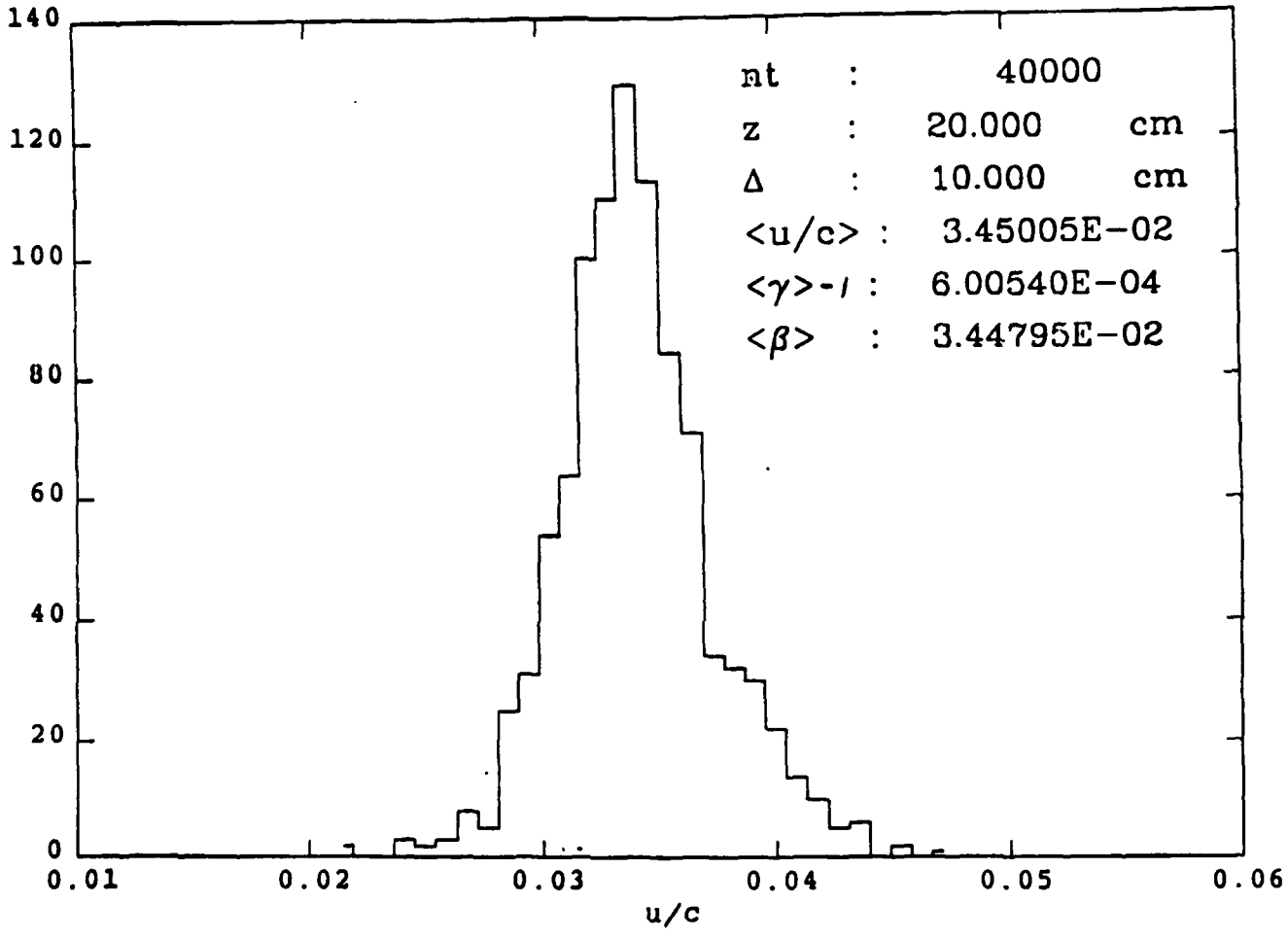
140
120
100
80
60
40
20
0
0.01
0.02
0.03
0.04
0.05
0.06
u/c
nt : 40000
z : 20.000 cm
Δ : 10.000 cm
<u/c> : 3.45005E-02
<γ>-1 : 6.00540E-04
<β> : 3.44795E-02

FIG. 3b

10 Papers and Presentations Resulting from this Research

The following papers, wholly or partly derived from this contract, were presented:

1. R.L. Yao, C.D. Striffler and J. Guillory, "Intense beam propagation and collective ion acceleration in a Localized plasma source-vacuum system," IEEE Int Conf. on Plasma Sci., June 1-3, 1987, Crystal City, VA.

2. R.L. Yao, C.D. Striffler and J. Guillory, "Collective Ion Acceleration, Intense Beam Propagation, and Plasmoid Emission in a Localized Plasma Source-Vacuum System," APS-DPP Meeting, Sand Diego, CA, November 2-6, 1987 [Bull. APS 32, 1719 (1987)].

3. R.L. Yao, C.D. Striffler and J. Guillory, "Numerical Simulation of Intense Beam Propagation and Plasmoid Formation in a Localized Plasma-Source and Vacuum System," IEEE Int. Conf. on Plasma Science, Seattle, WA, June 6-8, 1988; also APS-DPP Meeting, Hollywood, FL, October 31-November 4, 1988 [Bull. APS 33, 1955 (1988)].

4. W.W. Destler, J. Rodgers, Z. Segalov, C.D. Striffler, R.L. Yao, J. Guillory, and X. Zhang, "Review of Intense Electron Beam Transport in Gases," Proceedings, Int. Conf. BEAMS '88, Karlsruhe, W. Germany, July 4-8, 1988.

5. J. Guillory, R.L. Yao, C.D. Striffler and M. Reiser, "University of Maryland Plasmoid Program: Formation and Stability of Partially-Neutralized Plasma Clumps - Plasmoid Formation Concepts," DOE Plasmoid Workshop at SAIC, McLean, VA, October 18-19, 1988.

6. J. Guillory, "Interaction of a Partially Neutralized Hot-Electron Plasmoid with Low-Density Background Plasma - Preliminary Theory," APS-DPP Meeting, Hollywood, FL, November 4, 1988 [Bull. APS 33, 2118 (1988)].

7. J. Guillory and R.L. Yao, "Theory of Ionization of Gas by a Pulsed Reflexing Electron Beam - Loss of Stability," APS-DPP Meeting, Anaheim, CA, November 13-17, 1989 [Bull. APS **34**, 2103 (1989)].

8. R.L. Yao and C.D. Striffler, "Numerical Simulation of Collective Ion Acceleration in an Intense Electron Beam – Localized Gas Cloud System," J. Appl. Phys. **67**, 1650-1658 (1990). [Copy attached.]

9. J. Guillory, R. Yao, C.D. Striffler, and M. Reiser, manuscript in final stages of preparation for submission to a refereed journal, "Formation and Stability of Partially-Neutralized Plasma Clumps."

Numerical simulation of collective ion acceleration in an intense electron beam–localized gas cloud system

R. L. Yao and C. D. Striffler
Laboratory for Plasma Research and Department of Electrical Engineering, University of Maryland, College Park, Maryland 20742

(Received 5 September 1989; accepted for publication 7 November 1989)

In experiments in which an intense relativistic electron beam is injected into an evacuated drift tube with a localized gas cloud located near the anode, ions with energies several times the electron beam energy have been observed. These experiments have been simulated using a particle-in-cell code which realistically models ionization of the gas. It was found that when the injected electron beam current exceeds the space-charge limiting current, ions are accelerated to energies several times the electron beam energy by coherent motion of the ions and the intense virtual cathode electric fields. The dependence of the peak ion energy on the system parameters as observed in the simulations is also discussed. For the parameter regimes investigated with beam energies up to 3 MV, beam currents up to 35 kA, gas pressures up to 600 mTorr, and gas cloud widths up to 6 cm, peak ion energies of 5–6 times the electron beam energy have been observed.

I. INTRODUCTION

Because the electric fields produced by an intense relativistic electron beam (IREB) are much larger than those that can be attained in conventional accelerators, considerable work has been devoted to using IREBs to accelerate ions to high energies. In 1970, Graybill and Uglum[1] reported that ions with peak energies of four times the electron beam energy were produced when an IREB was injected into a gas-filled drift tube. In 1973, Luce, Sahlin, and Crites[2] reported that ions with energies several times the electron beam energy were produced when an IREB was injected into an evacuated drift tube using a diode with a dielectric insert in the anode. Since these results were published, collective ion acceleration has been reported for many other systems, including those in which the ions are produced by beam ionization of dielectric drift tube walls[3] or by laser ionization of a solid target.[4]

Recently, Destler, Floyd, and Reiser[5] reported that in experiments performed at the University of Maryland collective ion acceleration was observed when an IREB was injected into an evacuated drift tube after gas had been puffed into the drift tube through a nozzle located near the anode. A diagram of the University of Maryland experiment is shown in Fig. 1. The system consists of a foilless electron beam diode, a grounded cylindrical drift tube, a nozzle located near the anode through which gas is puffed into the drift tube, and magnetic field coils, which produce a guide field for the electron beam. In a typical experiment, the drift tube is first pumped down to vacuum (5×10^{-5} Torr). The puff value connected to the nozzle is then fired, injecting neutral gas into the drift tube through the nozzle and producing a cloud of gas extending no more than a few cm from the anode. The diode is then fired, injecting the beam into the drift tube through the cloud of gas. Current collectors placed at the downstream end of the drift tube measure the ion current and stacked-foil neutron activation analysis is used to determine the ion energy and flux.

In the experiments, it was found that when the injected current I_0 exceeded the space-charge limiting current I_L for the system, ions were accelerated to energies several times the electron beam energy V_0. For example, using a 1.5-MeV, 35-kA electron beam, protons were accelerated to energies of greater than 8 MeV (5.3 V_0/nucleon) and xenon ions were accelerated to energies of greater than 638 MeV (4.9 V_0/nucleon).[6] It was also found that the maximum ion energy was essentially independent of the applied magnetic field.[7]

The space-charge limiting current for a system is the maximum current that can be propagated through the system before the potential depression produced by the space-charge exceeds the beam energy. When the injected current exceeds the space-charge limiting current, a virtual cathode forms where the potential equals the beam energy. The fraction of the injected current which exceeds the space-charge limiting current is reflected by the virtual cathode back through the anode or deflected to the drift tube wall. For a solid beam of radius R_b in a cylindrical drift tube of radius R_w with a large focusing magnetic field, the space-charge limiting current is given by the formula[8]

$$I_L = \frac{17\,000(\gamma_0^{2/3}-1)^{3/2}}{1+2\ln(R_w/R_b)} - (\text{Amps}), \tag{1}$$

where γ_0 is the Lorentz factor for the injected electrons and where it is assumed that $R_b \ll R_w$.

Many explanations have been offered for collective acceleration in both gas-filled systems and evacuated systems. Among the first models to be proposed for collective ion acceleration in a gas-filled drift tube was that of Olson.[9] According to this model, which is based on work by Poukey and Rostoker,[10] collective ion acceleration occurs only when the current exceeds the space-charge limiting current. Soon after the electron beam is injected, the beam front stops near the anode, forming a stationary potential well with a depth of two to three times the electron beam energy. As the space charge near the anode is neutralized by ionization of the gas, the beam front and the potential well suddenly start to prop-

 0021-8979/90/041650-09$03.00

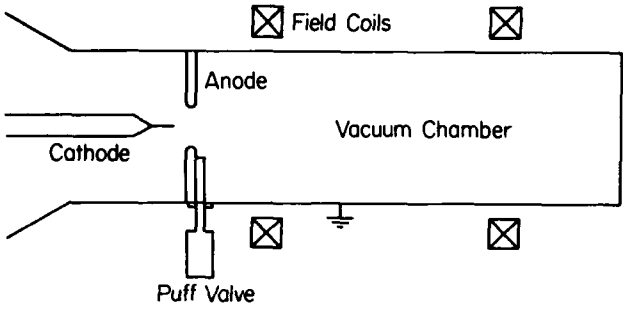

FIG. 1. Schematic of experimental setup for University of Maryland collective acceleration experiments.

agate downstream. Ions are accelerated by the deep, stationary potential well and by the moving potential well. This theory accounts for many of the experimental observations of collective ion acceleration in gas-filled systems and is consistent with some 2-D particle simulations of IREB injection into a neutral gas.[11]

The energies that are typically observed in evacuated systems such as the Luce diode configuration are much too high to be explained by the theory of Olson. Furthermore, Adler, Nation, and Serlin[12] have also reported detailed observations of collective ion acceleration in a Luce diode configuration which indicate that ion acceleration was not produced by a deep potential well or by a moving potential well at the beam front. They suggested instead that ions were accelerated by electrostatic waves which are driven by the two-stream instability. Destler *et al.*[4] suggested that in evacuated systems collective acceleration occurs by a bootstrap process. The early part of the beam pulse forms a dense plasma near the anode. If the beam current exceeds the space-charge limiting current and the plasma density is sufficiently high, a virtual cathode forms at the downstream edge of the plasma. The intense virtual cathode electric fields draw ions out of the plasma, the ions neutralize the electron beam space charge, and the virtual cathode moves further downstream. As this process is repeated, the beam electrons transfer momentum to the ions until the ions attain the same velocity as the beam-front electrons. A similar model was proposed earlier by Ryutov and Stupakov[13] for collective ion acceleration produced by injection of an IREB through a dense plasma layer. Mako and Tajima[14] modified the model using data obtained from experiments with a gas-filled drift tube, and were able to recover the experimentally measured peak ion energy (ten times the electron beam energy) and ion distribution. They also used a particle code to simulate injection of an IREB into an evacuated drift tube with a dense plasma layer located next to the injection plane. The simulations showed that the peak ion energies were limited by phase instability of the ions and the accelerating electric fields. However, using an artificially low ion mass, they also found that the peak ion energies never exceeded three times the electron beam energy and that, when the ion mass was doubled, the ion velocity decreased inversely as the square root of the mass. Using a 2-1/2-D electromagnetic particle code with a realistic ion mass, Faehl and Peter[15] and Peter *et al.*[16] simulated the same system and found that the virtual cathode formed at the downstream edge of the plasma layer soon after the beam was injected and that no subsequent motion of the virtual cathode occurred. They also pointed out that no such motion should be expected because the maximum ion current that can be extracted from the plasma is never large enough to neutralize the electron beam space charge. They suggested that collective acceleration is the result of ambipolar expansion of the plasma rather than motion of the virtual cathode.

In simulations of injection of an IREB from a plasma into free space, Chang and Reiser[17] found that as ions were extracted from the surface of the plasma by the virtual cathode electric fields, the location of the virtual cathode minimum shifted downstream from its initial location. They also observed ions which had been accelerated to energies approximately twice the electron beam energy and proposed that the coherent motion of the virtual cathode and the ions as the virtual cathode shifts downstream to its final position was responsible for accelerating the ions.

In this paper we present a detailed picture of the acceleration mechanism in the University of Maryland experiments, in which an intense relativistic electron beam is injected into an evacuated drift tube with a localized gas cloud located near the anode. We have obtained this picture using particle-in-cell (PIC) code simulations which realistically model ionization of the neutral gas.

Our simulations differ from previous simulations of collective acceleration in the following respects. In our simulations, an IREB is injected into an evacuated drift tube with a well-localized gas cloud located next to the anode, as opposed to a gas-filled drift tube or an evacuated drift tube with a plasma layer located next to the anode. Ions are produced in the drift tube by realistically modeling ionization of the gas by impact ionization, as opposed to assuming an initial distribution of ions or injecting ions. Realistic ion masses are also used. The finite radius of the beam is also taken into account, so that the simulations are more realistic than strictly 1-D simulations. Finally, the IREB is injected into a grounded drift tube rather than free space so that inductive effects can confidently be neglected. (We also note that our code is simple enough to permit a detailed investigation of the acceleration mechanism.)

In our simulations, we find that when the injected electron current exceeds the space-charge limiting current, a virtual cathode forms near the anode plane soon after the beam is injected. Neutralization of the electron beam space charge by impact ionization of the neutral gas then causes the virtual cathode to move downstream to the end of the gas region, where the virtual cathode stops. As the virtual cathode moves through the gas, ions are accelerated to energies several times the electron beam energy by the coherent motion of the ions and the intense virtual cathode electric fields. (This picture is similar to the mechanism observed by Chang and Reiser.)

Before proceeding, we would like to point out that the general features of the above picture are similar to results which have been obtained earlier at the University of Maryland.[18] The present work has also been extended to simulate enhanced collective ion acceleration in a laser-controlled

us, drift tube length, neutral gas pressure, and gas cloud width. We present a picture of the collective acceleration mechanism that we have observed in all of the simulations in which collective acceleration occurred. To do so, we will use the results of a single simulation. (We note that the parameter values differ from typical parameter values in the University of Maryland experiments. However, simulations performed with the experimental parameter values show that the acceleration mechanism is the same as described here.)

In the simulation, a 15-kA, 500-keV, 0.5-cm-radius electron beam is injected into a 4-cm-radius, 40-cm-long drift tube with a 1-cm-wide, 450-mTorr hydrogen cloud located next to the anode plane. The beam current and beam energy are assumed to rise instantaneously. According to Eq. (1), the space-charge limiting current for the system is approximately 1.4 kA. The time step is approximately 0.75 ps and the grid cell width is approximately 0.2 mm.

Figure 3 shows the time-integrated proton energy spectrum 7.5 cm from the anode plane 11 ns after the start of the run. The energy spectrum can be roughly divided into two parts—the bulk of the spectrum, which is centered about 0.6 MeV, and a tail that extends out to 1.5 MeV (three times the electron beam energy). We ignore the ions in the bulk of the spectrum and focus on the ions in the high-energy tail. Note that since the potential depression at the center of the drift tube is approximately -500 kV, the ion spectrum that would be observed by a grounded detector would be the same as the spectrum shown in Fig. 3 shifted to the left by 0.5 MeV. In the following, we present a detailed picture showing how the ions in the high-energy tail are accelerated to energies exceeding the electron beam energy.

In Fig. 4, the potential ϕ on axis near the anode plane is plotted as a function of distance z from the anode plane at several different time steps. About 40 ps after the start of the run, a virtual cathode forms about 2 mm from the anode plane, and the current measured downstream from the virtual cathode falls to a value approximately equal to the space-charge limiting current. After formation of the virtual cathode, the potential remains essentially the same for several thousand time steps (the position and amplitude of the virtual cathode oscillate in time at the local plasma frequency, but the time-averaged position and amplitude are approximately the same). The potential for time step 4600, which is shown in Fig. 4, is typical for this stage. During this stage, the beam electrons ionize the neutral gas, producing a plasma in the vicinity of the virtual cathode. The intense electric fields near the virtual cathode quickly expel the plasma electrons from the plasma region. The plasma ions are also accelerated by these electric fields but leave the plasma region at a much slower rate than the plasma electrons. They also tend to be accelerated downstream, whereas the plasma electrons tend to be accelerated upstream, where they exit from the drift tube through the anode plane. As plasma ions drift through the gas, they also contribute to the ionization. As the ion density in the plasma region increases, the virtual cathode moves downstream to the end of the plasma region leaving behind a positive potential region (time steps 4600–5000). Ions lying to the left of the peak of the positive potential are accelerated upstream and exit the drift tube through the anode plane. Ions lying to the right of the peak of the positive potential are accelerated downstream. As the ions move downstream, the virtual cathode also moves downstream with the positive potential region widening and extending downstream behind it (time steps 5000–5600). The virtual cathode ceases to move when it reaches the end of the gas region at $z = 1$ cm (time step 5600). We will see that ions are accelerated to energies of nearly 1.5 MeV during the time that the virtual cathode and the positive potential region move downstream.

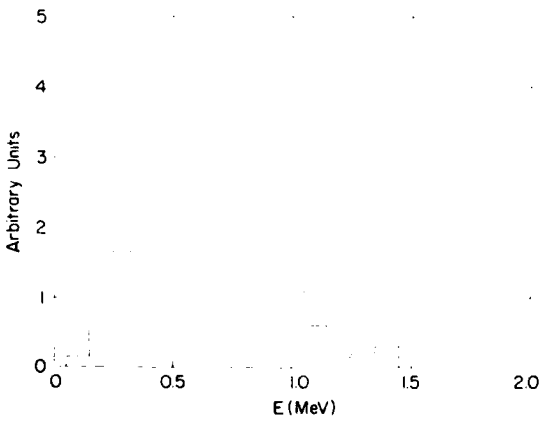

FIG. 3. Time-integrated proton energy spectrum at $z = 7.5$ cm after 11 ns. The run parameters are $I_0 = 15$ kA, $V_0 = 500$ keV, $R_b = 0.5$ cm, $R_w = 4$ cm, $d = 40$ cm, $p_0 = 450$ mTorr, and $z_0 = 1$ cm.

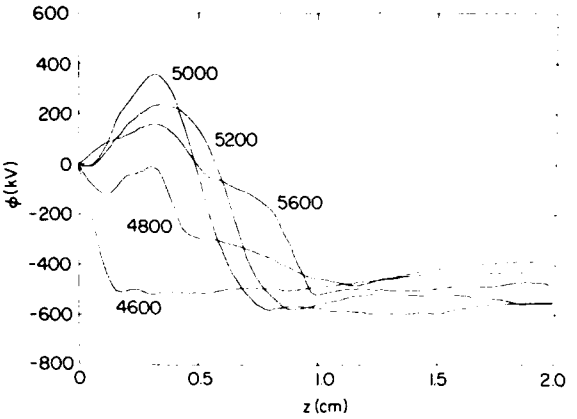

FIG. 4. Potential on axis ϕ near anode plane vs distance from anode plane z for time steps 4600, 4800, 5000, 5200, and 5600 during acceleration phase. Note that 1000 time steps equals about 0.75 ns. See Fig. 3 for system parameters.

The formation of a positive potential region has been observed experimentally and in other simulations.[14] The reason the potential in the plasma region becomes positive can be understood as follows. Because the electron impact ionization cross section peaks at low energies, the majority of ions are formed near the virtual cathode. The buildup of ions in the vicinity of the virtual cathode causes the beam electrons to spend more time there, and as a result the electron density downstream from the virtual cathode decreases. Hence, when the ion density is sufficiently high, the position of the virtual cathode can no longer be maintained and the virtual cathode begins to move downstream. (In fact, our

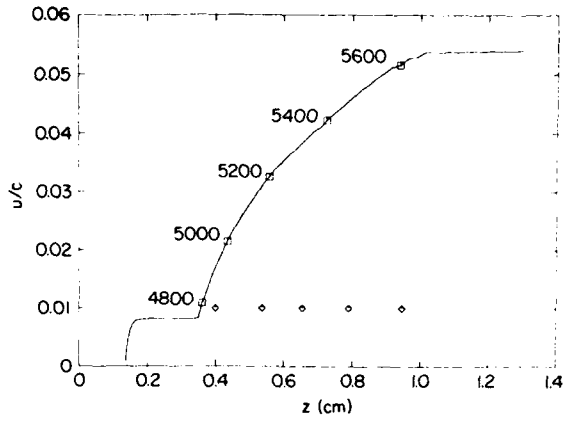

FIG. 5. Phase-space trajectory of collectively accelerated proton. The boxes plotted along the trajectory indicate the location of the ion at equally spaced time steps during the acceleration phase. The diamonds plotted along the base of the trajectory indicate the location of the peak electric field at the same time steps. See Fig. 3 for system parameters.

simulations show that immediately preceding the onset of the acceleration process, the electron current measured immediately downstream from the plasma region falls abruptly.) As the virtual cathode moves through the plasma region, the electrons behind the virtual cathode travel through the plasma with essentially the same speed with which they are injected. The increase in the speed of the electrons through the plasma region produces a sudden drop in the electron density. Hence, the virtual cathode leaves a net positive space charge in its wake and the potential becomes positive in the plasma region.

In Fig. 5, the phase-space trajectory of a collectively accelerated proton is shown during the collective acceleration process. The ion is created with zero velocity at a distance of about 1.3 mm from the anode plane about 2.6 ns after the start of the run (time step 3500). It is rapidly accelerated by the electric field near the virtual cathode to a velocity of about $0.008c$ (corresponding to an energy of 30 keV) and begins to drift downstream. When it has drifted about 2 mm downstream, the potential begins to go positive (at around time step 4700) and the virtual cathode begins to move downstream. As the virtual cathode moves downstream and the positive region extends downstream behind it (time steps 4800–5600), the proton is rapidly accelerated to a final velocity of about $0.054c$ (corresponding to an energy of 1.4 MeV).

The boxes plotted along the proton phase-space trajectory indicate points along the trajectory which are separated by equal time intervals of 200 time steps or about 150 ps. Each box is labeled with the corresponding time step starting with time step 4800. Below the phase-space trajectory, we have also plotted the location of the peak electric field at the same time steps. The peak electric field is always located in the region where the potential drops sharply from the edge of the positive potential region to the virtual cathode. As the virtual cathode moves downstream and the positive potential region extends downstream behind the virtual cathode the peak electric field also moves downstream. As can be seen from the figure, the ion follows closely behind the peak electric field for time steps 4800 to 5600. It is this coherent motion of the ion and the peak electric field through the plasma region which enables the ion to be accelerated to energies several times the energy it would gain if the potential were stationary.

Note that the trajectory of the proton in Fig. 5 is similar to the trajectory of an ion being accelerated by a constant electric field $v_z(z) = \sqrt{v_{z0}^2 + 2(eE_z/m_p)z}$, where v_{z0} is the initial ion velocity. Using values obtained from the figure in the above formula, we find that the electric field E_z is about 200 MV/m, which is near the peak virtual cathode electric field of 250 MV/m.

The reason for the coherent motion of the ion and the peak electric field during the motion of the potential front can be understood by considering the free expansion of a slab of ions, which initially has uniform density. As the slab expands, an ion at the surface of the slab always feels the same electric field, that is, the ion and the electric field travel at the same velocity. We believe that the same effect occurs during motion of the potential front. In the simulations, the ions at the front of the accelerated ion beam are accelerated not only by the space charge produced by the ions following behind but also by the electric field produced by the virtual cathode which always moves in front of the ion beam—the ions are pushed ahead by the ions which follow and simultaneously pulled ahead by the virtual cathode.

The reason the potential front stops moving at the end of the gas region can also be understood by considering the free expansion of a slab of ions. As the slab expands, the ion density and the potential decrease uniformly. In the gas region, ionization of the gas, particularly by ions, can supply ions at a rate sufficiently high to prevent total collapse of the potential and reformation of a virtual cathode near the anode. Beyond the gas region, no ions are produced and the ion density is too low to permit the virtual cathode to move forward. (As Faehl and Peter[15] observed, the maximum ion current which can be extracted from the plasma is space-charge limited and hence ions can never be extracted at a rate sufficient to significantly neutralize the electron beam space charge downstream.)

Although all of the collectively accelerated ions are accelerated by the moving potential front, some ions continue to accelerate, although at a much lower rate, after they have left the gas region. This additional acceleration is probably produced by the interaction of the collectively accelerated ions among themselves—interactions between ions that have been collectively accelerated in a bunch will cause ions with velocities greater than the mean velocity to be accelerated and ions with velocities less than the mean velocity to be decelerated.

Several bursts of accelerated ions, which follow one another at short intervals. are often observed in simulations. The multiple bursts are produced when the positive potential region collapses after the ions have been accelerated out of the gas region, the virtual cathode retreats to a location inside the gas region and the acceleration process repeats itself. If the pressure is increased, with all other system parameters kept constant, the multiple bursts are suppressed, probably because the rate of ion production in the gas region is suffi-

cient to prevent collapse of the positive potential region. Such multiple bursts have been observed in some experiments in evacuated systems.[12]

IV. RESULTS OF PARAMETER STUDIES

A. Dependence on beam energy and current

In Fig. 6, the peak proton energy E_{max} measured at $z = 7.5$ cm in the first 10 ns of the run is plotted as a function of the injected beam current I_0 for beam energies V_0 of 0.5, 1.0, 1.5, and 3.0 MeV. In each case, the gas pressure is 600 mTorr and the gas cloud width is 1 cm. Generally, E_{max} increases with beam current and beam energy. In Fig. 7, the same data are plotted with E_{max} normalized to V_0 and I_0 normalized to the space-charge limiting current I_L, given by Eq. (1). Notice that all the plotted points lie on approximately the same curve. For all values of V_0 which were used, no collectively accelerated protons are observed for $I_0/I_L < 1$. As I_0/I_L increases above unity, E_{max} increases sharply and then continues to increase but at a much slower rate. (Note that for fixed I_0, the ratio I_0/I_L decreases with increasing V_0. Hence for the same current I_0, the ratio E_{max}/V_0 with $V_0 = 0.5$ MeV is much larger than the ratio for $V_0 = 3$ MeV.)

The observed dependence of the peak proton energy on beam energy and current can be understood quite simply by recalling that the strength of the peak electric field increases with V_0 and I_0/I_L. In Fig. 8(a), the phase-space trajectories of collectively accelerated protons are shown for three different values of the injected current—10, 20, and 30 kA—and the same beam energy of 0.5 MeV. In each case, the gas pressure is 600 mTorr and the gas cloud width is 1 cm. Recalling that the accelerating electric field is approximately proportional to the product of the velocity u and the slope du/dz of the trajectory, it can be seen that as the current increases so does the accelerating electric field. In Fig. 8(b), the phase-space trajectories of collectively accelerated protons are shown for three different values of the beam energy—0.5, 1.0, and 1.5 MeV—and the same beam current of 30 kA. It can be seen that as the beam energy increases so does the accelerating electric field. (This dependence is not so clear when the trajectories for 0.5 and 1.0 MeV are compared, which illustrates the complex nature of the acceleration process, that is, the final ion energy depends not only on the strength of the electric field but also on the location and velocity of the ion when the virtual cathode begins to move downstream and on the velocity with which the virtual cathode moves.)

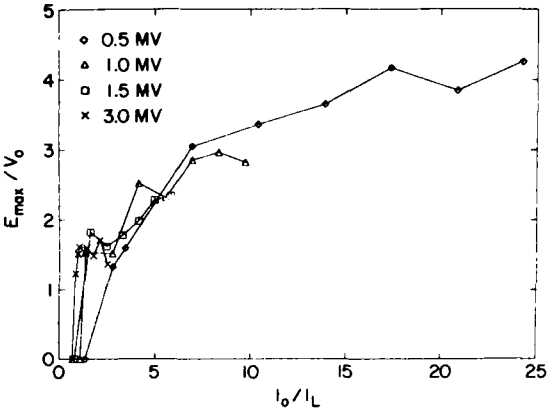

FIG. 7. Peak proton energy E_{max} normalized to beam energy V_0 vs injected current I_0 normalized to space-charge limiting current I_L. See Figs. 3 and 6 for system parameters.

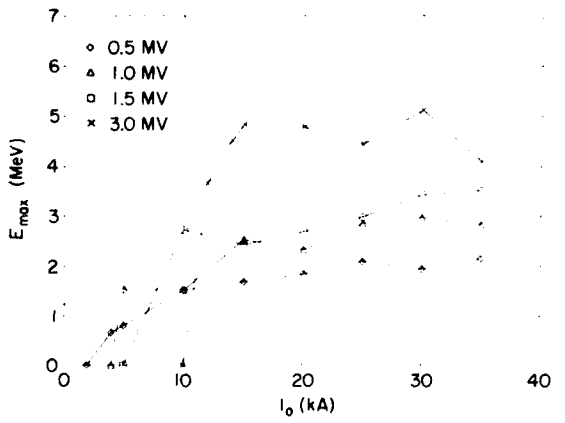

FIG. 6. Peak proton energy E_{max} measured at $z = 7.5$ cm in the first 10 ns vs injected current I_0 for $p_0 = 600$ mTorr, $z_0 = 1$ cm, and $V_0 = 0.5$, 1.0, 1.5, and 3.0 MeV. See Fig. 3 for system parameters.

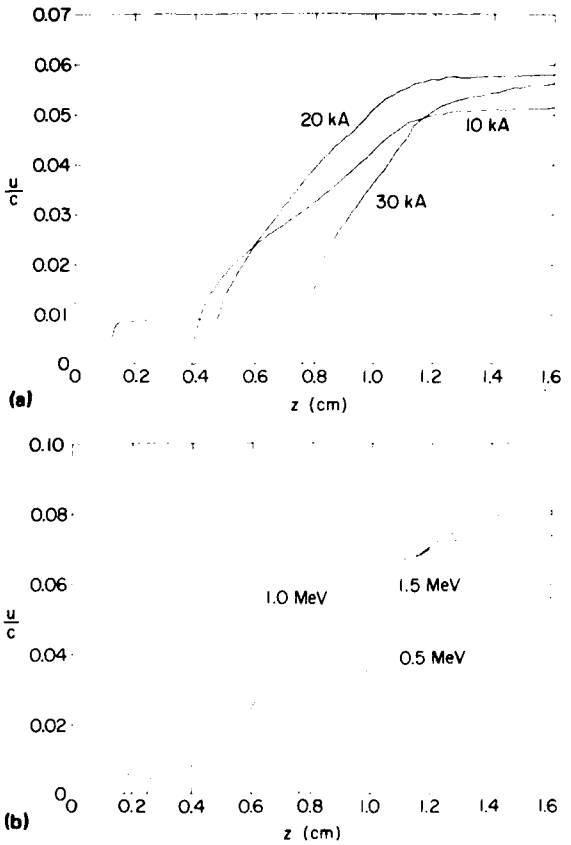

FIG. 8. Phase-space trajectories of collectively accelerated protons for (a) $V_0 = 0.5$ MeV and $I_0 = 10$, 20, and 30 kA, and for (b) $I_0 = 30$ kA and $V_0 = 0.5$, 1.0, and 1.5 MeV. See Fig. 3 for other system parameters.

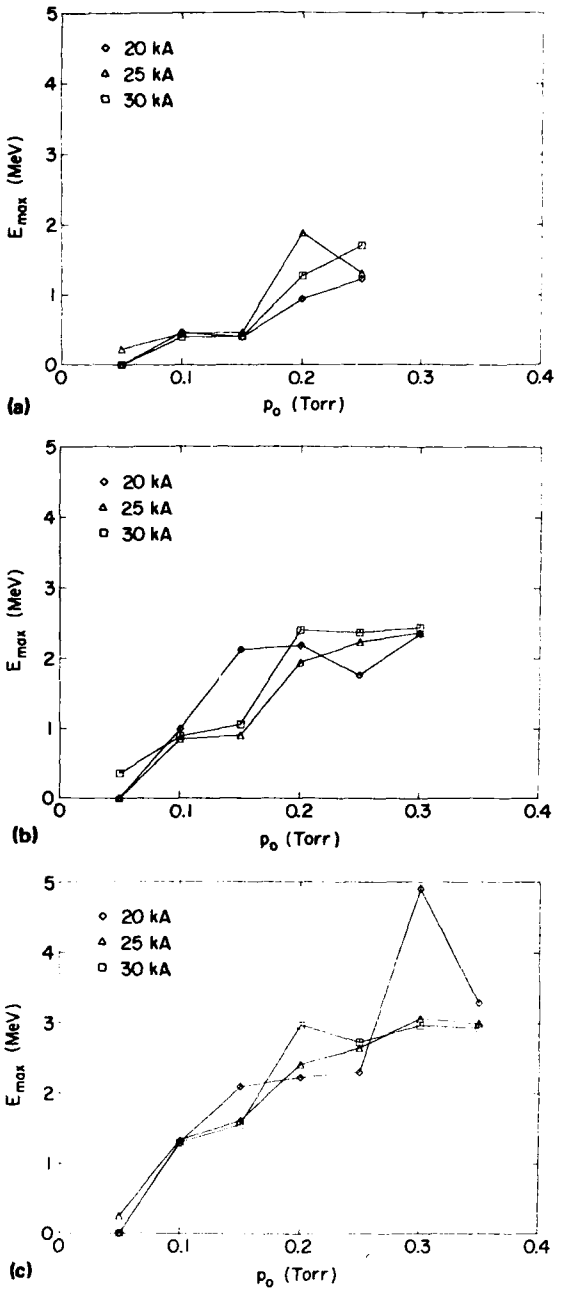

FIG. 9. Peak proton energy E_{max} measured at $z = 7.5$ cm after 20 ns vs gas pressure p_0 for $z_0 = 1$ cm and $V_0 =$ (a) 0.5, (b) 1.0, and (c) 1.5 MeV. See Fig. 3 for other system parameters.

B. Dependence on gas cloud pressure

In Fig. 9, the peak proton energy E_{max} measured at $z = 7.5$ cm in the first 20 ns of the beam pulse is plotted as a function of gas pressure p_0 for injected beam currents I_0 of 20, 25, and 30 kA and for beam energies V_0 of (a) 0.5, (b) 1.0, and (c) 1.5 MeV. In each case, the gas cloud width is 1.0 cm. At 50 mTorr, no collectively accelerated protons are observed in the first 20 ns of the beam pulse. Above 50 mTorr, E_{max} tends to increase with increasing pressure and level off at energies several times the electron beam energy. Generally, the higher the beam energy, the higher the energy and pressure at which the energy levels off.

The observed dependence of the peak proton energy on the pressure can be explained qualitatively as follows. At low pressures, the amount of ionization at the end of 20 ns is too small to neutralize the electron beam space charge and the virtual cathode remains at its initial position; no collective acceleration occurs and the peak proton energies which are measured are less than the electron beam energy. As the pressure is increased, the amount of ionization which is produced during the beam pulse becomes large enough to neutralize the electron beam space charge and permit the virtual cathode to move downstream. As it moves downstream, the virtual cathode electric fields accelerate ions to energies several times the electron beam energy. Once the acceleration process has begun, the final energy of a collectively accelerated ion depends only on the magnitude of the accelerating electric field and the distance over which the ion travels coherently with the electric field. Now, the magnitude of the electric field will be determined mainly by the electron beam energy and current and the density of ions in the plasma region at the start of the acceleration process (because the electric field at the surface of a slab of ions is proportional to the ion density in the slab). But the ion density at the start of the acceleration process is independent of the pressure, because it is proportional to the electron beam density, which is determined by the electron beam energy and current only. The only effect of increasing the gas pressure will be to decrease the time required for the ion density to build up before the acceleration process begins (which is in fact observed in simulations). Hence, the peak ion energy will depend only weakly on the neutral gas pressure, once the gas pressure is sufficiently high to cause collective acceleration.

The above picture is somewhat too simplistic because the gas pressure also affects the motion of the virtual cathode electric fields through the gas cloud. Generally, as the pressure increases, the virtual cathode moves through the gas cloud more quickly and higher peak proton energies are observed because the virtual cathode electric fields are able to accelerate the protons over a longer distance.

Although the dependence of collective acceleration on pressure as observed in our simulations is consistent with the model for collective acceleration which we have presented above, it disagrees with the experimental results obtained at the University of Maryland. In particular, Floyd *et al.*[6] reported that when a 1.5-MeV, 35-kA, 30-ns beam pulse was injected into a 25-cm-diam drift tube with a well-localized gas cloud located near the anode, collective acceleration was observed only in a narrow pressure window. In our simulations, we observe no such pressure window. In particular, we observe collective acceleration at all pressures up to 1 Torr.

The disagreement may have the following causes. First, in our simulations we have neglected charge exchange between protons and H_2 molecules. Since the mean free path for charge exchange for protons in H_2 is approximately 1 cm at 100 mTorr at approximately 100 keV,[9] at pressures of a few 100 mTorr charge exchange probably prevents acceleration of protons to energies much greater than a few 100 keV. Second, in our simulations we have neglected sources of ionization such as photoionization and prepulse ionization which could produce sufficient ionization in the gas region

to prevent formation of a virtual cathode near the injection plane. In simulations of injection of an IREB into vacuum with a localized plasma located next to the injection plane,[15,16,21] it was found that for plasma densities comparable to or exceeding the beam density, the virtual cathode formed near the downstream edge of the plasma. Finally, the disagreement with the reported experiments may be the result of changes in the electron beam diode characteristics as the pressure is increased. In the experiments, the peak gas cloud pressure at the time of beam injection was varied by simply varying the time delay between firing of the gas puff valve and firing of the diode. It was also found that when the gas puff was fired too early, the diode shorted out.[4]

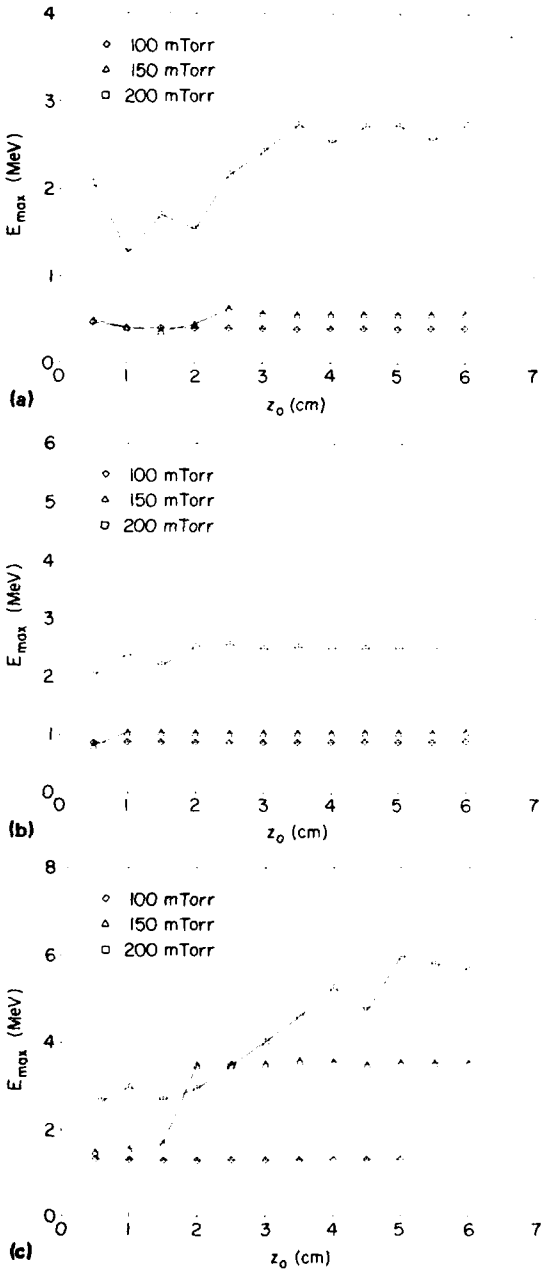

FIG. 10. Peak proton energy E_{max} measure at $z = 7.5$ cm after 20 ns vs gas cloud width z_0 for $I_0 = 30$ kA, $p_0 = 100$, 150, and 200 mTorr, and $V_0 =$ (a) 0.5, (b) 1.0, and (c) 1.5 MeV. See Fig. 3 for other system parameters.

C. Dependence on gas cloud width

In Fig. 10, the peak proton energy E_{max} measured at $z = 7.5$ cm in the first 20 ns of the beam pulse is plotted as a function of gas cloud width z_0 for electron beam energies V_0 of (a) 0.5, (b) 1.0, and (c) 1.5 MeV and several neutral gas pressures p_0. In each case, the injected electron beam current is 30 kA.

Figure 10 shows that E_{max} tends to increase with gas cloud width and then level off, and that this tendency becomes more pronounced as the pressure increases. In Fig. 10(c), for example, which shows data obtained for $V_0 = 1.5$ MeV, E_{max} increases approximately linearly with increasing gas cloud width before leveling off at about 6.0 MeV at $z_0 = 5.0$ cm for $p_0 = 200$ mTorr. (When $p_0 = 100$ mTorr, no collectively accelerated protons are detected in the first 20 ns of the beam pulse.)

The tendency of E_{max} to increase with increasing gas cloud width is consistent with the simple picture of collective acceleration presented above. Protons are accelerated to higher energies as the gas cloud width is increased because they are accelerated over longer distances. This trend is more pronounced at higher pressures because, as noted in the last section, higher pressures enable the virtual cathode to move through the gas cloud more quickly. Closer examination of the simulation results shows that E_{max} tends to increase as the gas cloud width increases because the protons are indeed accelerated over longer distances. Figure 11 shows the phase-space trajectories of two collectively accelerated ions for the same beam energy and current (30 kA) and the same gas cloud pressure (200 mTorr) but different gas cloud widths. It is clear from the figure that one proton is accelerated to a higher energy because it is accelerated over a longer distance. The figure also illustrates the reason for the tendency of the peak proton energy to level off as the gas cloud width is increased—the ions tend to outrun the moving potential front as it moves through the gas cloud (seen in the 3-cm case).

Results of simulations performed with different values of the injected beam current I_0 indicate that the value at which E_{max} levels off also tends to increase with beam current, although the correlation is relatively weak. In Fig. 12,

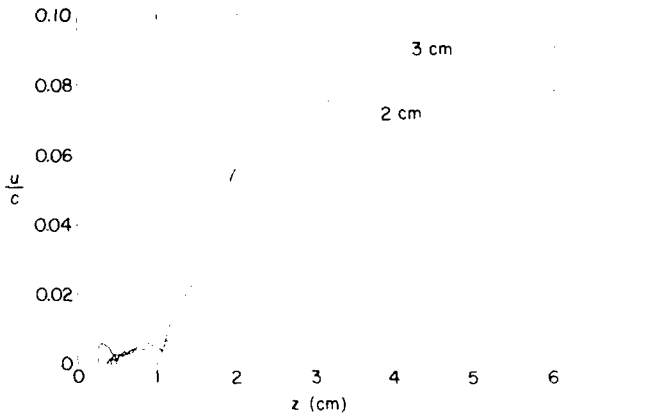

FIG. 11. Phase-space trajectory of collectively accelerated proton for $V_0 = 1.5$ MeV, $I_0 = 30$ kA, $p_0 = 200$ mTorr, and $z_0 = 2$ and 3 cm. See Fig. 3 for other system parameters.

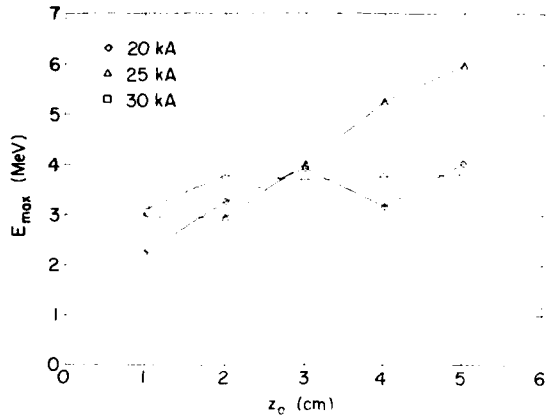

FIG. 12. Peak proton energy E_{max} measured at $z = 7.5$ cm after 20 ns vs gas cloud width z_0 for $V_0 = 1.5$ MeV, $p_0 = 200$ mTorr, and $I_0 = 20$, 25, and 30 kA. See Fig. 3 for other system parameters.

for example, the peak proton energy measured at $z = 7.5$ cm in the first 20 ns of the beam pulse is plotted as a function of gas cloud width for a beam energy of 1.5 MeV, a gas pressure of 200 mTorr, and injected beam currents of 20, 25 and 30 kA.

V. SUMMARY

In order to investigate collective ion acceleration observed in experiments in which an intense relativistic electron-beam is injected into an evacuated drift tube with a localized gas cloud located near the anode, we have written a relativistic, electrostatic PIC code that realistically models ionization of the gas.

Using the code, we have developed a simple model for the collective acceleration mechanism in these experiments. In this model, ionization of the gas causes the virtual cathode to move downstream through the gas cloud. As the virtual cathode moves through the gas cloud, ions are accelerated to energies several times the electron-beam energy by coherent motion of the ions and the intense virtual cathode electric fields.

Using the code, we have also determined the dependence of the peak ion energy on the system parameters, including the beam energy V_0, beam current I_0, the gas cloud pressure p_0, and the gas cloud width z_0. We find that the peak energy E_{max} tends to increase with increasing values of beam energy V_0 and beam current I_0. In particular we find that E_{max}/V_0 tends to increase as I_0/I_L, where I_L is the space-charge limiting current given by Eq. (1), and that the functional dependence is nearly the same for a wide range of parameters. We also find that as the pressure is increased, E_{max} jumps from a value approximately equal to the beam energy to a value several times the beam energy, and that generally, the higher the beam energy, the higher the pressure at which E_{max} reaches the final energy. We also find that, generally, E_{max} tends to increase with gas cloud width z_0 and then level off when z_0 is a few cm and that this tendency is more pronounced for higher pressures. Our results indicate that the mechanism for collective acceleration which we have observed in our simulations can produce protons with energies of at least 5–6 times the electron beam energy when the beam and the gas cloud properties are optimized.

ACKNOWLEDGMENTS

We would like to acknowledge useful discussions with W. W. Destler, M. P. Reiser, and M. J. Rhee. Research sponsored by DOE and AFOSR.

[1] S. E. Graybill and J. R. Uglum, J. Appl. Phys. **41**, 236 (1970).
[2] J. S. Luce, H. L. Sahlin, and T. R. Crites, IEEE Trans. Nucl. Sci. **NS-20**, 336 (1973).
[3] A. Greenwald and R. Little, in *Collective Methods of Acceleration*, edited by N. Rostoker and M. Reiser (Harwood Academic, New York, 1979), p. 371; J. A. Pasour, R. K. Parker, R. L. Gullickson, W. O. Doggett, and D. Pershing, *ibid.*, p. 383; A. V. Agafonov, A. A. Kolomensky, E. G. Krastelev, A. N. Lebedev, and B. N. Yablokov, *ibid.*, p. 395.
[4] W. W. Destler, H. S. Uhm, H. Kim, and M. Reiser, J. Appl. Phys. **50**, 3015 (1979).
[5] W. W. Destler, L. E. Floyd, and M. Reiser, Phys. Rev. Lett. **44**, 70 (1980).
[6] L. E. Floyd, W. W. Destler, M. Reiser, and H. M. Shin, J. Appl. Phys. **52**, 693 (1981).
[7] L. E. Floyd and W. W. Destler, J. Appl. Phys. **57**, 1592 (1985).
[8] L. S. Bogdankevich and A. A. Rukhadze, Sov. Phys. Usp. **14**, 163 (1971).
[9] C. L. Olson and V. Schumacher, *Collective Ion Acceleration* (Springer, New York, 1979).
[10] J. W. Poukey and N. Rostoker, Plasma Phys. **13**, 897 (1971).
[11] J. W. Poukey and C. L. Olson, Phys. Rev. A **11**, 691 (1975).
[12] R. Adler, J. A. Nation, and V. Serlin, Phys. Fluids **24**, 347, (1981).
[13] D. D. Ryutov and G. V. Stupakov, Sov. J. Plasma Phys. **2**, 309 (1976).
[14] F. Mako and T. Tajima, Phys. Fluids **27**, 1815 (1984).
[15] R. J. Faehl and W. K. Peter, IEEE Trans. Nucl. Sci. **NS-32**, 3500 (1985).
[16] W. Peter, R. J. Faehl, C. Snell, and M. E. Jones, IEEE Trans. Nucl. Sci. **NS-32**, 3506 (1985).
[17] C. R. Chang and M. Reiser, J. Appl. Phys. **61**, 899 (1987).
[18] J. M. Grossman, R. Kulkarni, C. D. Striffler, and R. J. Faehl, Proceedings of the Ninth Conference on Numerical Simulation of Plasmas, June 30–July 2, 1980, Northwestern University, Evanston, IL; J. M. Grossman, I. Mayergoyz, and C. D. Striffler, IEEE Trans. Nucl. Sci. **NS-28**, 2587 (1981); C. D. Striffler and H. Dantsker, Bull. Am. Phys. Soc. **27**, 983 (1982); H. Dantsker, L. E. Floyd, and C. D. Striffler, Bull. Am. Phys. Soc. **29**, 1353 (1984).
[19] R. L. Yao, W. W. Destler, C. D. Striffler, J. Rodgers, and Z. Segalov, Proceedings of the 1989 Particle Acceleration Conference, March 20–23, 1989, Chicago, IL.
[20] W. W. Destler, R. J. Faehl, M. Reiser, P. G. O'Shea, Z. Segalov, C. D. Striffler, and X. Zhang, Proceedings of the Sixth International Conference on High-Power Particle Beams, June 9–12, 1986, Kobe, Japan, p. 215; W. W. Destler, J. Rodgers, Z. Segalov, C. D. Striffler, R. L. Yao, X. Zhang, and J. Guillory, Proceedings of the Seventh International Conference on High-Power Particle Beams, July 4–8, 1988, Karlsruhe, W. Germany, p. 185.
[21] M. Galvez and G. Gisler, Preprint LA-UR-88-1160, Los Alamos National Laboratories.